

EFFICIENT AND ROBUST NEURAL COMBINATORIAL OPTIMIZATION VIA WASSERSTEIN-BASED CORESETS

Anonymous authors

Paper under double-blind review

ABSTRACT

Combinatorial optimization (CO) is a fundamental tool in many fields. Many neural combinatorial optimization (NCO) methods have been proposed to solve CO problems. However, existing NCO methods typically require significant computational and storage resources, and face challenges in maintaining robustness to distribution shifts between training and test data. To address these issues, **first**, we model CO instances into probability measures, and introduce Wasserstein-based metrics to quantify the difference between CO instances. **Then**, we leverage a popular data compression technique, *coreset*, to construct a small-size proxy for the original large dataset. However, the time complexity of constructing a coreset is linearly dependent on the size of the dataset. Consequently, it becomes challenging when datasets are particularly large. **Next**, we accelerate the coreset construction by adapting it to the merge-and-reduce framework for achieving parallel computing. Additionally, we prove that our coreset is a good representation in theory. **Subsequently**, to speed up the training process for existing NCO methods, we propose an efficient training framework based on the coreset technique. We train the model on a small-size coreset rather than on the full dataset, and thus save substantial computational and storage resources. Inspired by hierarchical Gonzalez’s algorithm, our coreset method is designed to capture the diversity of the dataset, which consequently improves robustness to distribution shifts. **Finally**, experimental results demonstrate that our training framework not only enhances robustness to distribution shifts but also achieves better performance with reduced resource requirements.

1 INTRODUCTION

Combinatorial optimization (CO) is a fundamental tool in many fields such as transportation (Conrado et al., 2012; Veres & Moussa, 2019), logistics (Laterre et al., 2018) and manufacturing (Froger et al., 2016; Dolgui et al., 2019; Liu et al., 2017). Numerous traditional exact (David Applegate, 2006; Optimization, 2020) or heuristic solvers (Croes, 1958; Helsgaun, 2017; Lamm et al., 2016) have been designed by experts to solve these problems. However, the real-world CO problems are widespread and diverse, and may even undergo rapid changes over time. Moreover, even for a fixed CO problem, human experts may be hindered by limited domain knowledge and computational difficulty (many of these CO problems are NP-hard). As a result, in many situations, it can be impractical to rely solely on hand-crafted methods developed by experts.

To address these challenges, numerous *Neural Combinatorial Optimization* (NCO) methods have been proposed, such as constructive heuristics methods (Khalil et al., 2017; Kool et al., 2018; Kwon et al., 2020; Hottung et al., 2020; Kim et al., 2022; Joshi et al., 2019; Fu et al., 2021; Geisler et al., 2021; Qiu et al., 2022; Sun & Yang, 2023; Luo et al., 2023; Vinyals et al., 2015; Bello et al., 2016; Nazari et al., 2018; Deudon et al., 2018; Xin et al., 2020, 2021; Kwon et al., 2021; Kim et al., 2021; Cheng et al., 2023; Drakulic et al., 2023) and improvement heuristics methods (Li et al., 2018; d O Costa et al., 2020; Wu et al., 2021; Chen & Tian, 2019; Li et al., 2023; Chen & Tian, 2019; Hottung et al., 2020; Joshi & Anand, 2022; Joshi et al., 2019). These methods learn heuristic solution strategies in a data-driven manner, thus dispensing with laborious manual design and expert knowledge; moreover, compared with traditional CO solvers, NCO methods can benefit from accelerated inference speeds by utilizing modern GPU devices.

Despite their advantages, these methods often require large training datasets, which demands substantial storage space and computational resources. Additionally, when training data and test data come from different distributions, enhancing the robustness to distribution shift (Liang et al., 2023; Sun et al., 2020) is also a challenge for existing NCO models. Therefore, training a competitive model with limited resources while ensuring its robustness to distribution shifts is an important and worthy problem to address.

To address these issues, we consider constructing a good representation, *coreset* (Ros & Guillaume, 2020), for the original huge dataset. Coreset is a popular data compression technique, which can accelerate the training process by reducing dataset size while preserving the value. Roughly speaking, coreset is a small-size proxy of the original dataset \mathcal{Q} with respect to an objective; the value of the objective evaluated on coreset can closely approximate the value evaluated on \mathcal{Q} . Therefore, we can replace \mathcal{Q} by coreset in the training phase, and thus save the storage space and computational resources significantly. Furthermore, our coreset method is inspired by hierarchical Gonzalez’s algorithm (Gonzalez, 1985), and thus can capture the diversity of the dataset. Consequently, benefiting from its diversity, the model based on our coreset method shows robustness to distribution shift.

The intuition behind our coreset technique can be likened to preparing for an exam. Training neural networks is similar to practicing exercises for an exam. While the number of available exercises (i.e., data) might be vast, we cannot be trained for all the exercises with limited time and energy (i.e., storage and computational resources). Fortunately, the whole exercises are redundant; to get a high score, doing all the exercises is unnecessary, and we only need to cover all categories of exercises. Based on the above intuitions, we need a small-size representation (i.e., coreset) for the whole exercises. To this end, three key steps are required: i) exploring a proper metric to quantify the difference between CO instances; ii) constructing a coreset for the original dataset; iii) designing an efficient training framework based on the coreset technique for existing NCO models.

Many CO problems, such as the Traveling Salesperson problem (TSP) and Maximum Independent Set (MIS), can inherently induce a graph structure. By employing graph embedding techniques, we can map these graph structures into a set of points in Euclidean space. Thus, we model CO instances as probability measures (in section 3.1). Wasserstein distance is commonly used to quantify the difference between probability measures. However, solutions to CO problems like TSP remain invariant under rigid transformations such as translation, rotation, and reflection. In other words, a CO instance can generate multiple variants through these transformations; but, they are inherently the same instance. Therefore, the distance between such instances should be zero. To capture this property, we introduce the Wasserstein distance under rigid transformations (RWD) to measure the difference between two CO instances.

Our contributions:

- First, we model CO instances as probability measures, and introduce RWD to quantify the difference between two given CO instances.
- Then, based on RWD, we design a coreset algorithm to effectively compress data for training acceleration; it saves substantial computational and storage resources. However, the time required to construct the coreset increases linearly with the size of the dataset, making it computationally expensive for extremely large datasets.
- To further accelerate coreset construction, we adapt our coreset method to merge-and-reduce framework, enabling parallel computation. Furthermore, to accelerate the coreset construction process, to enable parallel computing. Moreover, we demonstrate that our coreset is a good representation theoretically.
- Next, based on our coreset method, we propose an efficient training framework for accelerating the existing NCO training process. More specifically, we replace the original dataset with our coreset to accelerate the training process; in the inference phase, test instances are aligned along our tree (i.e., \mathcal{T} from Algorithm 1 or 2) before predicting their labels using the trained model.
- The experimental results show that our training framework exhibits better performance and enhanced robustness to distribution shifts.

1.1 OTHER RELATED WORKS

Here, we introduce several techniques that will be involved later.

Graph embedding technique represents the nodes and edges of a graph in Euclidean space. The edge information is encoded within the Euclidean distances between points, reducing the need to handle complex graph structures directly, as point-to-point information suffices. Moreover, it transforms the discrete graph into continuous Euclidean coordinates, which allows many techniques in Euclidean space to be used. Here are some widely used graph embedding methods. Laplacian Eigenmaps (Belkin & Niyogi, 2001) embed graph data into a low-dimensional Euclidean space while preserving local neighborhood relationships. Multidimensional Scaling (MDS) (Borg & Groenen, 2007) focuses on preserving pairwise distances between nodes in the graph. Isomap (Tenenbaum et al., 2000) extends MDS by incorporating geodesic distances along the manifold, making it especially useful for graphs with inherent nonlinear structures.

Hierarchical Gonzalez’s algorithm (Murtagh & Contreras, 2012) is a variant of Gonzalez’s k -center algorithm for addressing hierarchical clustering problem. In this approach, clusters are recursively divided or merged at different levels of granularity, yielding a tree structure for efficient querying. This algorithm prioritizes selecting new center points that are far apart from the previously chosen ones. This strategy leads to clusters well-spread across the data, effectively capturing the diversity of the dataset. This method is commonly used for summarizing large datasets. However, its time complexity exhibits a linear dependence on the size of the dataset, making it potentially time-consuming for extremely large datasets. To mitigate this issue, we integrate merge-and-reduce (Bentley & Saxe, 1980; Har-Peled & Mazumdar, 2004) technique to construct our coreset in Algorithm 2.

2 PRELIMINARIES

Notations We define $[n] := \{1, \dots, n\}$ and denote the vector of ones by $\mathbf{1}$. The ℓ_2 -norm is denoted by $\|\cdot\|$, and $|A|$ denotes the size of set A . Let \mathbb{R}_+ be the set of non-negative real numbers. Let $\mathcal{P}(\mathbb{R}^d)$ be the probability measure space on Euclidean space \mathbb{R}^d . Matrices are denoted by bold capital letters, such as \mathbf{C} ; C_{ij} is its element in the i -th row and j -th column. Similarly, we denote vectors by bold lowercase letters, such as $\mathbf{a} := (a_1, \dots, a_n)^T \in \mathbb{R}^n$; a_i is its i -th element.

Wasserstein distance (Peyré et al., 2017) is skilled at capturing the geometric structures of CO problems, but it is sensitive to rigid transformations. To obtain the invariance property under rigid transformations, we consider the following conception: *Wasserstein distance under rigid transformation (RWD)*.

Definition 2.1 (RWD). Let $\mu = \sum_{i=1}^n a_i \delta_{x_i}$, $\nu = \sum_{j=1}^n b_j \delta_{y_j} \in \mathcal{P}(\mathbb{R}^d)$, where $\mathbf{a}, \mathbf{b} \in \mathbb{R}_+^n$ are their weight vectors and $\{x_i\}_{i \in [n]}, \{y_j\}_{j \in [n]} \subset \mathbb{R}^d$ are their locations. Then, the Wasserstein distance under rigid transformation between μ and ν is

$$\mathcal{W}(\mu, \nu) := \left(\min_{\mathbf{P} \in \Pi(\mathbf{a}, \mathbf{b}), e \in E(d)} \sum_{i=1}^n \sum_{j=1}^n P_{ij} \|x_i - e(y_j)\|^2 \right)^{1/2},$$

where $\Pi(\mathbf{a}, \mathbf{b}) := \{\mathbf{P} \in \mathbb{R}_+^{n \times n} \mid \mathbf{P}\mathbf{1} = \mathbf{a}, \mathbf{P}^T\mathbf{1} = \mathbf{b}\}$ is the coupling set, $E(d)$ is the euclidean group on \mathbb{R}^d , and $e : \mathbb{R}^d \rightarrow \mathbb{R}^d$ is the rigid transformation.

Remark 2.2. i) If we fix e as identity transformation, then RWD is degenerated as the Wasserstein distance; Wasserstein distance is a metric on $\mathcal{P}(\mathbb{R}^d)$. ii) RWD is a (semi-)metric¹ on $\mathcal{P}(\mathbb{R}^d)$; more specifically, $(\mathcal{P}(\mathbb{R}^d), \mathcal{W})$ is a metric space.

Next, we formally define our coreset technique. Let

$$\ell : \mathcal{Q} \times \Theta \rightarrow \mathbb{R}_+, \quad (\mu, \theta) \mapsto \ell(\mu, \theta) \quad (1)$$

be a loss function, where $\theta \in \Theta$ is the model parameter and $\mu \in \mathcal{Q}$ denotes a CO instance. For any weighted set $A \subset \mathcal{Q}$ with weight function w_A , we define $\ell(A, \theta) := \sum_{\mu \in A} w_A(\mu) \cdot \ell(\mu, \theta)$.

¹For simplicity, we do not distinguish between metric and semi-metric.

Definition 2.3 (Coreset). Let $0 < \epsilon < 1$ and ℓ be a loss function. Let $\mathcal{Q} \subset \mathcal{P}(\mathbb{R}^d)$ be a set of measures with weight function $w_{\mathcal{Q}} : \mathcal{P}(\mathbb{R}^d) \rightarrow \mathbb{R}_+$. Let $\sum_{\mu \in \mathcal{Q}} w_{\mathcal{Q}}(\mu) = 1$. Then, a weighted set \mathcal{S} with weight function $w_{\mathcal{S}}$ is an ϵ -coreset of \mathcal{Q} if

$$\ell(\mathcal{S}, \theta) \in (1 \pm \epsilon) \cdot \ell(\mathcal{Q}, \theta) \quad \text{for all } \theta \in \Theta. \quad (2)$$

Then, we introduce some basic properties that will be used later. *Doubling dimension* (Chan et al., 2016) can describe the growth rate of the dataset with respect to some metric dist . Formally, the doubling dimension of metric space $(\mathcal{Q}, \text{dist})$ is the smallest positive integer ddim such that every ball in $(\mathcal{Q}, \text{dist})$ can be covered by 2^{ddim} balls of half the radius. For example, the doubling dimension of the Euclidean space \mathbb{R}^d is $\Theta(d)$.

The Lipschitz constant of a function describes how fast it can change. The loss function is L -Lipschitz continuous with respect to dist on \mathcal{Q} , if $|\ell(\mu_1, \theta) - \ell(\mu_2, \theta)| \leq L \cdot \text{dist}(\mu_1, \mu_2)$ holds for all $\mu_1, \mu_2 \in \mathcal{Q}, \theta \in \Theta$.

3 OUR METHODS

This section introduces our methods. Section 3.1 introduces RWD to quantify the difference between two CO instances. Section 3.2 constructs a small-size coreset for accelerating the training process. Section 3.3 accelerates coreset construction process by using merge-and-reduce framework; moreover, we theoretically demonstrate that our coreset is a good representation. Finally, in Section 3.4, we present our efficient framework for existing NCO methods.

3.1 METRICS FOR CO INSTANCES

Many CO problems can induce graph structures. We first extract the graph structure induced by the CO instance and represents it by a graph metric space, where each point in this space reflects node-specific information, and edge relationships are captured through the corresponding shortest-path metric. We then apply graph embedding techniques (in Section 1.1) to map this graph metric space into Euclidean space, aiming to preserve inter-point distances closely. In this embedding, each node in the original graph is represented as a discrete point in Euclidean space, and edge information is encoded in Euclidean distances between these points. Ultimately, we represent the graph as a discrete set of points in Euclidean space. Henceforth, we focus on the point set data within the Euclidean space.

Given two CO instances, we represent the nodes of their corresponding graph structure as $X = \{x_i\}_{i \in [n]}, Y = \{y_j\}_{j \in [n]} \subseteq \mathbb{R}^d$. Then, the CO instances are modeled as two probability measures $\mu = \sum_{i=1}^n a_i \delta_{x_i}$ and $\nu = \sum_{j=1}^n b_j \delta_{y_j}$ (with $a_i = b_j = \frac{1}{n}$ to represent equal node importance). Then, we can quantify the difference between μ and ν with metric RWD; that is, $\mathcal{W}(\mu, \nu)$, where the ground distance between $x \in X$ and $y \in Y$ is $\|x - y\|$ as in Definition 2.1.

Remark 3.1. i) By graph embedding technique, the nodes and edges of a graph structure are described by the locations and their ground distances in Euclidean space. ii) These CO problems are usually invariant after imposing rigid transformations on their nodes, and RWD can capture this characteristic well. In essence, the complexity of data space is reduced under RWD metric. More specifically, we regard two CO instances as the same instance if their distance is zero. iii) The complete graph in \mathbb{R}^d can be represented directly by a point set, without the need for graph embedding techniques. iv) If we fixed the outer iteration number and the dimension d of data space as constants, our RWD can be solved within $\tilde{O}(n^2)$ time by using the heuristic in Algorithm 3.

3.2 CORESET

Intuitively, our coreset aims to cover all the data by using relatively fewer and smaller balls, where all the balls have the same radius. This strategy can be likened to preparing for an exam, where we need to cover as many categories of exercises as possible with limited time and energy. For simplicity, we take RWD as an example to illustrate our methods. The metric RWD can also be replaced by Wasserstein distance, or some other proper metrics on $\mathcal{P}(\mathbb{R}^d)$.

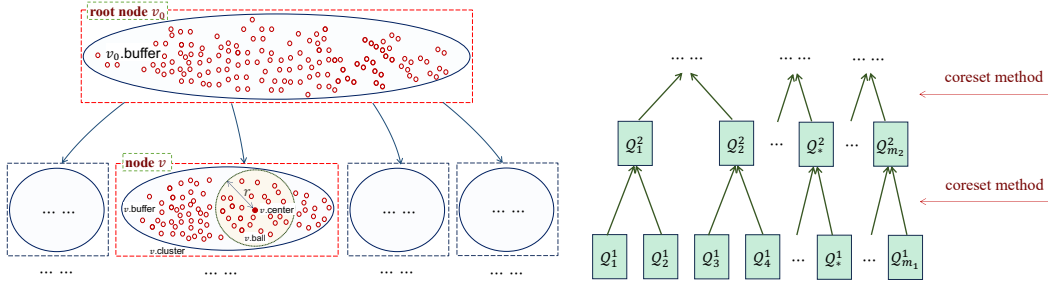


Figure 1: Grow nodes from root v_0 with $\text{ddim} = 2$. The red dot denotes probability measures in dataset \mathcal{Q} , and the solid red dot is the center of the ball $v.\text{ball}$.

Figure 2: Accelerate the coreset construction by using merge-and-reduce framework.

Coreset construction Our algorithm is inspired by the hierarchical structure in (Ding et al., 2021; Krauthgamer & Lee, 2004; Har-Peled & Mendel, 2005; Beygelzimer et al., 2006). Given a set \mathcal{Q} of probability measures, we aim at clustering similar measures into small balls of radius r , and take the cluster centers to form our coreset. The coreset is finally reserved in the tree \mathcal{T} as shown in Figure 1.

To construct such a coreset, we first initialize an empty tree \mathcal{T} , and set its root node as v_0 . The root node has only one attribute **buffer**, and is initialized as $v_0.\text{buffer} = \mathcal{Q}$. Our (non-root) node has four attributes: **cluster**, **center**, **buffer** and **ball** as shown in Figure 1. The nodes grow in an up-bottom manner recursively. Given a current node v , if $v.\text{buffer}$ is an empty set, then v is a leaf node, and we stop adding children to it. If $v.\text{buffer}$ is a nonempty set, we add $k = \min\{|v.\text{buffer}|, 2^{2-\text{ddim}}\}$ children node $\{v'_j\}_{j \in [k]}$ to the current node v ; more specifically, we run Gonzalez’s algorithm k rounds on $v.\text{buffer}$. By this, we obtain k cluster centers $v'_j.\text{center}$ and their corresponding clusters $v'_j.\text{cluster}$. All the $v'_j.\text{cluster}$ form a partition of $v.\text{buffer}$; each $v'_j.\text{cluster}$ consists of points that are relatively close to its center $v'_j.\text{center}$. For each set $v'_j.\text{cluster}$, we partition it into two sets $v'_j.\text{ball}, v'_j.\text{buffer}$, where $v'_j.\text{ball}$ is a RWD-based ball of radius r centered at measure $v'_j.\text{center}$; formally, we can formulate them as

$$v'_j.\text{ball} = \{\mu \in v'_j.\text{cluster} \mid \mathcal{W}(\mu, v'_j.\text{center}) \leq r\} \quad (3)$$

and

$$v'_j.\text{buffer} = v'_j.\text{cluster} - v'_j.\text{ball}. \quad (4)$$

Finally, we obtain a tree \mathcal{T} . The coreset \mathcal{S} consists of all the center points $v.\text{center}$ with weight $|v.\text{ball}|$. We show the coreset construction process in a more intuitive and comprehensible manner in Figure 1. The detailed descriptions are in Algorithm 1.

Algorithm 1 Algorithm for constructing coresets

Input: a set $\mathcal{Q} := \{\mu_i\}_{i \in [N]} \subset \mathcal{P}(\mathbb{R}^d)$ of measures, doubling dimension ddim of \mathcal{Q} , radius r

- 1: Initialize an empty tree \mathcal{T} , and set its root node as v_0 ;
- 2: Set $v_0.\text{buffer} = \mathcal{Q}$;
 \triangleright The root node v_0 only has an attribute **buffer**, and it is not associated with any node.
- 3: Construct the nodes of \mathcal{T} recursively as follows: $\triangleright v$ is the current node.
- 4: **if** $v.\text{buffer}$ is \emptyset **then**
- 5: The current node v is a leaf node, and we stop adding children to it;
- 6: **else**
- 7: Set $k = \min\{|v.\text{buffer}|, 2^{2-\text{ddim}}\}$ and add k children node $\{v'_j\}_{j \in [k]}$ to the current node v ;
- 8: Run Gonzalez’s algorithm k rounds on $v.\text{buffer}$. For each children node v'_j , we set its attributions **cluster**, **center**, **ball**, **buffer** according to Equation (3) and Equation (4);
- 9: **end if**
- 10: Set $\mathcal{S} = \{v.\text{center} \mid v \text{ is a node of } \mathcal{T}\}$ and set the weight as $w_{\mathcal{S}}(\mu) = |v.\text{ball}|$;

Output: \mathcal{T}, \mathcal{S}

Time complexity and coreset size From (Ding et al., 2021), we know that the radius of the clusters will be halved after carrying out at most $2^{2 \cdot \text{ddim}}$ rounds of Gonzalez’s algorithm. Let R be the radius of dataset \mathcal{Q} ; that is, $\mathcal{W}(\mu, \nu) \leq 2R$ for any $\mu, \nu \in \mathcal{Q}$. Thus, the height of the tree in Algorithm 1 is at most $\mathcal{O}(\log \frac{R}{r})$. Let $T(n)$ be the time for computing the distance (i.e., RWD) between two measures, where n is the size of the locations of measures. Since constructing every layer takes $\mathcal{O}(2^{2 \cdot \text{ddim}}) \cdot |\mathcal{Q}|$ computations of RWD, the total time complexity for Algorithm 1 is $\mathcal{O}(2^{2 \cdot \text{ddim}}) \cdot |\mathcal{Q}| \cdot T(n) \cdot \log \frac{R}{r}$. Its time complexity increases linearly with the size of the dataset, making it computationally expensive for large datasets. The coreset is maintained in the tree \mathcal{T} . The tree has $\mathcal{O}((2^{2 \cdot \text{ddim}})^{\log \frac{R}{r}})$ nodes, thus the coreset size is $\mathcal{O}((\frac{R}{r})^{2 \cdot \text{ddim}})$.

Remark 3.2. i) The output of Algorithm 1 contains a tree \mathcal{T} and coreset \mathcal{S} . The \mathcal{S} is a representation of the original measure set \mathcal{Q} , which is used for speeding up the training process for existing NCO methods; while the tree \mathcal{T} is prepared for aligning CO instances at the inference phase. ii) It is often not necessary to know the exact value of the doubling dimension in advance. Typically, we begin by experimenting with relatively small values, as demonstrated in our study where we set the low doubling dimension as $\text{ddim} = 1$. In practice, even if we cannot rigorously prove that the data satisfies low doubling dimension assumption, this generally does not impact the effectiveness of our experimental results. iii) All the v -ball consist of a partition of \mathcal{Q} .

3.3 ACCELERATE THE CORESET CONSTRUCTION PROCESS

In this subsection, we adapt our coreset method to merge-and-reduce framework (Bentley & Saxe, 1980; Har-Peled & Mazumdar, 2004; Wang et al., 2021); by this, we offer a technique to accelerate our coreset construction process by achieving parallel computing; moreover, it can also be used to tackle streaming data.

Algorithm 2 is a combination of our coreset method and the merge-and-reduce framework as shown in Figure 2. We first set $s = \mathcal{O}((\frac{R}{r})^{2 \cdot \text{ddim}})$, $H = \log_{\frac{r}{s}} \frac{|\mathcal{Q}|}{s}$ and $r' = \frac{r}{H}$. The height of the tree in Figure 2 is at most H , and it is generated in a bottom-up manner.

We perform reduce and merge procedures alternatively in each epoch. More specifically, *reduce* means data compression; that is, we run Algorithm 1 by taking $(\mathcal{Q}_i^h, \text{ddim}, r')$ as input, and obtain the corresponding coreset \mathcal{S}_i^h ; *merge* means putting together the coresets \mathcal{S}_i^h ; that is, $\mathcal{Q}^{h+1} = \cup_{i \in [m_h]} \mathcal{S}_i^h$. After H epochs, we obtain the coreset $\mathcal{S} = \mathcal{Q}^{H+1}$ and its corresponding tree $\mathcal{T} = \mathcal{T}^{H+1}$.

Algorithm 2 Algorithm for accelerating the coreset construction process

Input: a set $\mathcal{Q} := \{\mu_i\}_{i \in [N]} \subset \mathcal{P}(\mathbb{R}^d)$ of measures, doubling dimension ddim of \mathcal{Q} , radius r

- 1: Set $s = \mathcal{O}((\frac{R}{r})^{2 \cdot \text{ddim}})$, $H = \log_{\frac{r}{s}} \frac{|\mathcal{Q}|}{s}$ and $r' = \frac{r}{H}$, $\mathcal{Q}^0 = \mathcal{Q}$;
- 2: **for** $h = 1, \dots, H$ **do**
- 3: **▷ reduce procedure**
 Partition \mathcal{Q}^h as $\mathcal{Q}^h = \sqcup_{i \in [m_h]} \mathcal{Q}_i^h$ with $|\mathcal{Q}_i^h| = \mathcal{O}(\tau)$ and $m_h = \lceil \frac{|\mathcal{Q}^h|}{\tau} \rceil$;
 For every \mathcal{Q}_i^h , we run Algorithm 1 by taking $(\mathcal{Q}_i^h, \text{ddim}, r')$ as input, and output $(\mathcal{T}_i^h, \mathcal{S}_i^h)$;
- 4: **▷ merge procedure**
- 5: $\mathcal{Q}^{h+1} = \cup_{i \in [m_h]} \mathcal{S}_i^h$;
- 6: **end for**
- 7: Set $\mathcal{S} = \mathcal{Q}^{H+1}$ and $\mathcal{Q} = \mathcal{T}^{H+1}$;

Output: \mathcal{T}, \mathcal{S}

Time complexity Given that the input size of Algorithm 1 is $\mathcal{O}(\tau)$, and its output size is s . Then, the tree induced by the merge-and-reduce framework has at most $H = \log_{\frac{r}{s}} \frac{|\mathcal{Q}|}{s}$ layers.

Each layer of Algorithm 2 performs multiple computations of Algorithm 1 in parallel. Hence, the time complexity of per layer is $\tilde{\mathcal{O}}(2^{2 \cdot \text{ddim}} \cdot \tau \cdot T(n)) \cdot \log \frac{R}{r}$. Consequently, the overall time complexity of Algorithm 2 is $\tilde{\mathcal{O}}(2^{2 \cdot \text{ddim}} \cdot \tau \cdot T(n) \cdot \log \frac{R}{r} \cdot \log_{\frac{r}{s}} \frac{|\mathcal{Q}|}{s})$, which is independent on the dataset size.

Communication complexity Our coreset is a subset of the original dataset, allowing us to transmit only the indexes of the CO instance items rather than the data items themselves. This significantly reduces transmission costs. As a result, the additional transfer complexity introduced by our merge-and-reduce framework in Algorithm 2 is, in practice, minimal and unlikely to pose a substantial overhead.

Moreover, the coreset size of Algorithm 2 remains consistent with that in Algorithm 1, it is sufficient to retain only the tree structure of the final layer in practice.

A good representation Next, we show that the coreset \mathcal{S} is a good representation of the original huge dataset \mathcal{Q} in the following theorem.

Theorem 3.3. Assume ℓ is L -Lipschitz continuous on $(\mathcal{Q}, \text{RWD})$ and there exists a constant γ such that $\ell(\mathcal{Q}, \theta) \geq \gamma$ for all $\theta \in \Theta$. Let ddim be the doubling dimension of \mathcal{Q} with respect to RWD , and R be the radius of \mathcal{Q} . Then, by setting $r = \frac{\epsilon\gamma}{L}$, both Algorithm 1 and Algorithm 2 can generate an $\mathcal{O}((\frac{R}{r})^{2 \cdot \text{ddim}})$ size ϵ -coreset \mathcal{S} for the dataset \mathcal{Q} ; that is, for every θ , it holds that $\ell(\mathcal{S}, \theta) \in (1 \pm \epsilon) \cdot \ell(\mathcal{Q}, \theta)$.

It shows that for every parameter $\theta \in \Theta$, the value of the loss function ℓ evaluated on small-size coreset \mathcal{S} can approximate the value on the original dataset \mathcal{Q} within $\mathcal{O}(\epsilon)$ relative error. Therefore, Theorem 3.3 demonstrates that our small-size coreset \mathcal{S} is a good representation for the original huge dataset \mathcal{Q} with respect to the objective ℓ .

Proof. Due to limited space, we only give the proof sketch here. More details are in Appendix. First, we prove that by taking $(\mathcal{Q}, \text{ddim}, r)$ as input, the coreset constructed by Algorithm 2 can cover the dataset \mathcal{Q} by small balls of radius r by using mathematical induction. Then, we obtain that the value difference of the loss function between the data itself and its representation is small by Lipschitz continuous property. Third, by setting some parameters properly, we turn the additive error into a relative error and obtain an ϵ -coreset \mathcal{S} . \square

3.4 AN EFFICIENT FRAMEWORK

Here, we introduce an efficient framework to train a comparative model by using limited resources for existing NCO methods. We first feed the original dataset \mathcal{Q} into Algorithm 1 or Algorithm 2, and obtain the coreset \mathcal{S} and tree \mathcal{T} . The original dataset \mathcal{Q} is replaced by small-size coreset \mathcal{S} in the training phase. Thus, it saves the storage and computing resources significantly in the training phase. The probability measure μ in our coreset \mathcal{S} has its own weight $w_{\mathcal{S}}(\mu)$, which helps it represent the original dataset well. However, to capture the diversity better, we usually regard these data as equally important; that is, to improve the robustness to distribution shifts in experiments, we set their weights as $w_{\mathcal{S}} = \frac{1}{|\mathcal{S}|}$.

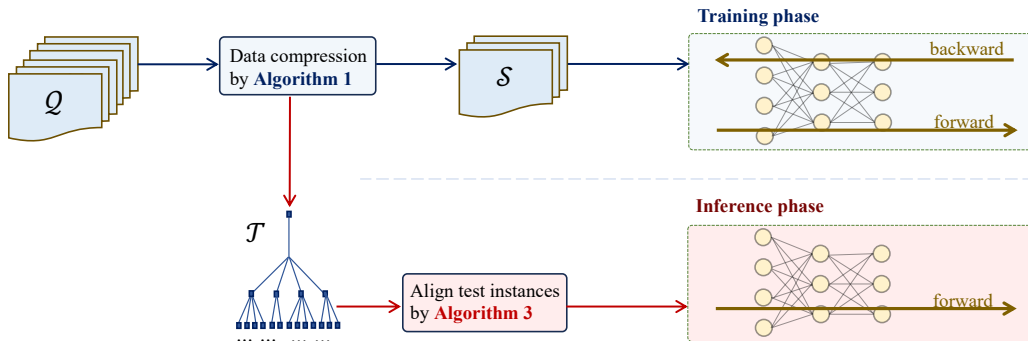


Figure 3: An efficient framework for accelerating existing NCO methods. The Algorithm 1 can be replaced by Algorithm 2, and Algorithm 4 is in Appendix.

Meanwhile, in the inference phase, we first align the test instances μ along our tree \mathcal{T} , which aims to find a rigid transformation such that

$$\min_{e, \nu} W(e(\mu), \nu) \text{ for all } \nu \in \mathcal{S}, \quad (5)$$

where $W(\cdot, \cdot)$ is the Wasserstein distance and $e(\mu) := \sum_{i \in [n]} a_i \delta_{e(x_i)}$ for any $\nu = \sum_{j \in [n]} b_j \delta_{y_j}$. We offer a heuristic method (i.e., Algorithm 4 in Appendix) for the alignment as described in Equation (5). Thanks to the tree structure maintained by \mathcal{T} , we can finish the alignment for a test instance within $\mathcal{O}(k \cdot \log(|\mathcal{S}|) \cdot T(n))$ time. This is particularly efficient in practice since k is usually small. Without this tree structure, we would potentially need to align the test instance with every training data, which could be significantly more time-consuming.

Remark 3.4. By combining our coreset technique in the training phase and the alignment process in the test phase, we essentially reduce the complexity of data. Intuitively, if the model can solve an instance well, then it can solve similar instances well under metric FWD. Furthermore, our framework can be applied to other problems that inherently involve a graph structure. This demonstrates its general applicability across various domains where graph-based analysis is pertinent.

Remark 3.5. i) Our coreset only needs to be computed once, after which it can be used repeatedly to train different models and fine-tune parameters. ii) Even if the coreset computation is time-consuming, it is still valuable as it helps save storage space. iii) Our alignment process before predicting their labels serves as an optional enhancement to improve performance rather than a mandatory step.

Table 1: Comparison of uniform sampling and our coreset method using TSP100-2D- $\mathcal{N}(0, 1)$ as the training dataset on test data TSP100-2D from different distributions.

Sample size	Method	Test distribution	Greedy		Greedy+2-opt	
			Length (\downarrow)	Time (\downarrow)	Length (\downarrow)	Time (\downarrow)
128000	Org	$\mathcal{N}(0, 1)$	20.39	386	18.61	384
		$\mathcal{N}(0, 4)$	76.41	374	67.39	388
		$\mathcal{U}(0, 10)$	89.29	372	79.82	385
4003	US	$\mathcal{N}(0, 1)$	22.34	378	18.92	387
		$\mathcal{N}(0, 4)$	101.95	379	69.28	395
		$\mathcal{U}(0, 10)$	119.78	380	82.59	395
	CS	$\mathcal{N}(0, 1)$	22.21	372	18.87	379
		$\mathcal{N}(0, 4)$	80.63	372	67.92	379
		$\mathcal{U}(0, 10)$	94.73	373	80.64	377
	CS-aligned	$\mathcal{N}(0, 1)$	22.18	359	18.88	363
		$\mathcal{N}(0, 4)$	80.66	362	67.91	358
		$\mathcal{U}(0, 10)$	94.94	361	80.53	360
	US	$\mathcal{N}(0, 1)$	22.12	377	18.87	388
		$\mathcal{N}(0, 4)$	83.17	377	68.13	378
		$\mathcal{U}(0, 10)$	97.31	377	80.80	387
8245	CS	$\mathcal{N}(0, 1)$	21.79	366	18.84	383
		$\mathcal{N}(0, 4)$	78.72	372	67.79	378
		$\mathcal{U}(0, 10)$	92.99	374	80.35	377
	CS-aligned	$\mathcal{N}(0, 1)$	21.80	360	18.86	359
		$\mathcal{N}(0, 4)$	78.50	361	67.82	358
		$\mathcal{U}(0, 10)$	93.04	355	80.42	361
	US	$\mathcal{N}(0, 1)$	21.99	390	18.87	377
		$\mathcal{N}(0, 4)$	80.78	384	67.94	379
		$\mathcal{U}(0, 10)$	95.01	369	80.60	379
12951	CS	$\mathcal{N}(0, 1)$	21.57	372	18.81	382
		$\mathcal{N}(0, 4)$	77.80	369	67.58	379
		$\mathcal{U}(0, 10)$	92.01	378	80.23	375
	CS-aligned	$\mathcal{N}(0, 1)$	21.50	361	18.79	358
		$\mathcal{N}(0, 4)$	77.67	362	67.57	357
		$\mathcal{U}(0, 10)$	92.01	358	80.21	359

4 EXPERIMENTS WITH TSP

We take TSP100 as an example to show the advantages of our coreset method. All experiments are conducted on a NVIDIA L20 GPU. Due to limited space, further experiments (including TSP training on uniformly sampled data (Kool et al., 2018), the MIS problem (Ahn et al., 2020)) and Capacitated Vehicle Routing Problem (CVRP) are presented in the Appendix.

Table 2: Comparison of uniform sampling and our coreset method using TSP100-2D- $\mathcal{N}(0, 1)$ as the training dataset on test data of varying sizes. We fix the sample size as 12951.

TSP size	Method	Test distribution	Greedy		Greedy+2-opt	
			Length (\downarrow)	Time (\downarrow)	Length (\downarrow)	Time (\downarrow)
TSP200	US	$\mathcal{N}(0, 1)$	33.69	109	27.14	112
		$\mathcal{N}(0, 4)$	125.99	108	96.70	112
		$\mathcal{U}(0, 10)$	145.41	109	113.39	112
	CS	$\mathcal{N}(0, 1)$	30.75	107	26.69	110
		$\mathcal{N}(0, 4)$	110.48	109	94.84	111
		$\mathcal{U}(0, 10)$	129.77	107	111.47	109
	CS-aligned	$\mathcal{N}(0, 1)$	30.77	77	26.68	79
		$\mathcal{N}(0, 4)$	110.99	78	94.59	79
		$\mathcal{U}(0, 10)$	129.28	76	111.4	9 78
	US	$\mathcal{N}(0, 1)$	59.81	1012	43.41	1020
		$\mathcal{N}(0, 4)$	237.72	1012	154.28	1022
		$\mathcal{U}(0, 10)$	263.66	1015	180.75	1022
TSP500	CS	$\mathcal{N}(0, 1)$	49.11	1012	42.25	1016
		$\mathcal{N}(0, 4)$	178.56	1010	149.50	1016
		$\mathcal{U}(0, 10)$	208.36	1011	174.93	1016
	CS-aligned	$\mathcal{N}(0, 1)$	49.38	680	42.26	683
		$\mathcal{N}(0, 4)$	178.88	679	149.63	682
		$\mathcal{U}(0, 10)$	208.77	678	175.03	682
	US	$\mathcal{N}(0, 1)$	94.71	2823	61.72	2848
		$\mathcal{N}(0, 4)$	382.77	4224	219.16	2847
		$\mathcal{U}(0, 10)$	426.61	4215	255.95	4254
	CS	$\mathcal{N}(0, 1)$	69.76	2823	59.59	2833
		$\mathcal{N}(0, 4)$	252.92	4224	210.71	2832
		$\mathcal{U}(0, 10)$	299.80	4215	246.57	4234
TSP1000	CS-aligned	$\mathcal{N}(0, 1)$	69.96	2825	59.57	2832
		$\mathcal{N}(0, 4)$	253.63	2821	210.81	2830
		$\mathcal{U}(0, 10)$	300.03	2812	246.61	2827

Dataset We apply our method on TSP100-2D/3D Euclidean instances. The labels of TSP100-2D instances are obtained by using the LKH-3 heuristic solver (Helsgaun, 2017); each coordinate of the nodes in a TSP instance is generated by $x\%10$, where x is randomly sampled either from a normal distribution $\mathcal{N}(0, \sigma^2)$ or uniform sampling $\mathcal{U}(0, 10)$. Our training data, TSP100-2D- $\mathcal{N}(0, 1)$ and TSP100-3D- $\mathcal{N}(0, 1)$, consists of 125,000 instances generated by the normal distribution $\mathcal{N}(0, 1)$ and 3000 instances by the uniform distribution $\mathcal{U}(0, 10)$. Indeed, the distribution of the training dataset is very close to the normal distribution $\mathcal{N}(0, 1)$. Hence, we regard the test data sampled from distribution $\mathcal{N}(0, 1)$ as having no distribution shift. The test data is sampled from a single distribution, either a normal distribution or uniform distribution. Specifically, we sample 1280 test data items for TSP100, and 128 test data items for other cases. Obviously, the uniform distribution has the highest entropy and thus the highest diversity. For these Gaussian distributions, the larger the variance, the larger the diversity.

As for the TSP100-3D dataset, we can directly extend the 2D instances to 3D instances by appending a third coordinate with a value of zero. Let $X = \{x_i\}_{i \in [n]} \subset \mathbb{R}^3$ are the nodes of an instance. We apply random rotation transformation e on X ; that is, $e(X) := \{e(x_i)\}_{i \in [n]}$. Intuitively, this TSP100-3D dataset has the same intrinsic complexity under metric RWD, which is the low doubling dimension in our assumption.

Setting We use the DIFUSCO (Sun & Yang, 2023) as our NCO solver. The detailed parameter settings are in Appendix. To quantify the performance of different methods, we use two criteria: the average tour length (Length) and the total runtime (Time). The term “Greedy” refers to the greedy decoding method of DIFUSCO, and “2-opt” is a post-processing used to improve solutions. The terms US, CS and CS-aligned represent uniform sampling, our coreset without alignment, and our coreset with alignment, respectively. We take the model trained on the full dataset with 128000 data items as baseline.

Table 3: Comparison of uniform sampling and our coreset method using TSP100-2D- $\mathcal{N}(0, 1)$ as the training dataset on test data TSPLIB(Reinelt, 1991).

Sample size	Method	Test distribution	Greedy		Greedy+2-opt	
			Length (\downarrow)	Time (\downarrow)	Length (\downarrow)	Time (\downarrow)
128000	Org	$\mathcal{N}(0, 1)$	129.35	108	112.23	106
	US	$\mathcal{N}(0, 1)$	190.79	109	115.87	108
	CS	$\mathcal{N}(0, 1)$	153.08	107	113.56	108
	CS-aligned	$\mathcal{N}(0, 1)$	152.70	103	113.71	105
8245	US	$\mathcal{N}(0, 1)$	166.40	106	114.47	108
	CS	$\mathcal{N}(0, 1)$	140.49	107	113.04	106
	CS-aligned	$\mathcal{N}(0, 1)$	140.18	104	112.91	104
	US	$\mathcal{N}(0, 1)$	162.19	107	114.31	107
12951	CS	$\mathcal{N}(0, 1)$	133.63	106	112.45	105
	CS-aligned	$\mathcal{N}(0, 1)$	133.14	103	112.52	110

Results of TSP100-2D Tables 1 to 3 present the results on training dataset TSP100-2D- $\mathcal{N}(0, 1)$. The training datasets are generated by the uniform sampling and our coreset technique respectively. The results show that both our method and uniform sampling method perform better as the sample size increases. Meanwhile, as the sample size decreases, the advantage of our methods compared to uniform sampling becomes increasingly evident.

Moreover, Tables 1 and 2 demonstrate that our method is robust to distribution shift. Specifically, the training data is sampled from a normal distribution $\mathcal{N}(0, 1)$, while the test data is sampled from normal distributions $\mathcal{N}(0, 1)$, $\mathcal{N}(0, 4)$ and a uniform distribution $\mathcal{U}(0, 10)$. The test distributions $\mathcal{N}(0, 4)$ and $\mathcal{U}(0, 10)$ are significantly different from the training distribution $\mathcal{N}(0, 1)$, which represent substantial distribution shifts. The results in Tables 1 and 2 show that our method consistently outperforms the baselines, demonstrating its robustness to distribution shifts.

Furthermore, Table 2 shows that models trained on our coreset can generalize better to larger problem sizes such as TSP200, TSP500 and TSP1000. Moreover, Table 3 confirms that our method outperforms other approaches on the TSPLIB dataset.

Results of TSP100-3D Tables 8 to 10 show the results on training dataset TSP100-3D- $\mathcal{N}(0, 1)$. For the test data without distribution shift (i.e., $\mathcal{N}(0, 1)$), our method has comparable performance; for the test data occurring distribution shift (i.e., $\mathcal{N}(0, 4)$ and $\mathcal{U}(0, 10)$), our method has better performance. Moreover, our coreset with alignment version performs better in the TSP-3D case. From Tables 1 to 3, 9 and 10, alignment can perform better for higher dimension dataset (i.e., TSP-3D). Thus, the alignment version is promising for tackling high-dimensional data. (The details are in Appendix.)

5 CONCLUSION AND FUTURE WORK

In this paper, we introduce an efficient training framework for NCO problems based on our coreset method. More specifically, we replace the original huge dataset with our coreset during the training phase. In the test phase, we first align the test instances with the data in our coreset, and then feed them into existing NCO models. Our framework enables the development of comparable models with limited computational and storage resources; additionally, it exhibits robustness to distribution shifts. Moreover, in future work, we will extend our method to other situations that can induce graph structures.

REFERENCES

- Sungsoo Ahn, Younggyo Seo, and Jinwoo Shin. Learning what to defer for maximum independent sets. In *International Conference on Machine Learning*, pp. 134–144. PMLR, 2020.
- Mikhail Belkin and Partha Niyogi. Laplacian eigenmaps and spectral techniques for embedding and clustering. *Advances in neural information processing systems*, 14, 2001.
- Irwan Bello, Hieu Pham, Quoc V Le, Mohammad Norouzi, and Samy Bengio. Neural combinatorial optimization with reinforcement learning. *arXiv preprint arXiv:1611.09940*, 2016.
- Jon Louis Bentley and James B Saxe. Decomposable searching problems i. static-to-dynamic transformation. *Journal of Algorithms*, 1(4):301–358, 1980.
- Alina Beygelzimer, Sham Kakade, and John Langford. Cover trees for nearest neighbor. In *Proceedings of the 23rd international conference on Machine learning*, pp. 97–104, 2006.
- Ingwer Borg and Patrick JF Groenen. *Modern multidimensional scaling: Theory and applications*. Springer Science & Business Media, 2007.
- Vladimir Braverman, Vincent Cohen-Addad, H-C Shaofeng Jiang, Robert Krauthgamer, Chris Schwiegelshohn, Mads Bech Tofttrup, and Xuan Wu. The power of uniform sampling for core-sets. In *2022 IEEE 63rd Annual Symposium on Foundations of Computer Science (FOCS)*, pp. 462–473. IEEE Computer Society, 2022.
- T-H Hubert Chan, Anupam Gupta, Bruce M Maggs, and Shuheng Zhou. On hierarchical routing in doubling metrics. *ACM Transactions on Algorithms (TALG)*, 12(4):1–22, 2016.
- Ke Chen. On coresets for k-median and k-means clustering in metric and euclidean spaces and their applications. *SIAM Journal on Computing*, 39(3):923–947, 2009.
- Xinyun Chen and Yuandong Tian. Learning to perform local rewriting for combinatorial optimization. *Advances in Neural Information Processing Systems*, 32, 2019.
- Hanni Cheng, Haosi Zheng, Ya Cong, Weihao Jiang, and Shiliang Pu. Select and optimize: Learning to solve large-scale tsp instances. In *International Conference on Artificial Intelligence and Statistics*, pp. 1219–1231. PMLR, 2023.
- Claudio Contardo, Catherine Morency, and Louis-Martin Rousseau. *Balancing a dynamic public bike-sharing system*, volume 4. Cirrelet Montreal, 2012.
- Georges A Croes. A method for solving traveling-salesman problems. *Operations research*, 6(6): 791–812, 1958.
- Marco Cuturi. Sinkhorn distances: Lightspeed computation of optimal transport. *Advances in neural information processing systems*, 26, 2013.
- Paulo R d O Costa, Jason Rhuggenaath, Yingqian Zhang, and Alp Akcay. Learning 2-opt heuristics for the traveling salesman problem via deep reinforcement learning. In *Asian conference on machine learning*, pp. 465–480. PMLR, 2020.
- Vasek Chvátal William Cook David Applegate, Robert Bixby. Concorde tsp solver. <https://www.math.uwaterloo.ca/tsp/concorde/index.html>, 2006.
- Michel Deudon, Pierre Cournut, Alexandre Lacoste, Yossiri Adulyasak, and Louis-Martin Rousseau. Learning heuristics for the tsp by policy gradient. In *Integration of Constraint Programming, Artificial Intelligence, and Operations Research: 15th International Conference, CPAIOR 2018, Delft, The Netherlands, June 26–29, 2018, Proceedings 15*, pp. 170–181. Springer, 2018.
- Hu Ding, Tan Chen, Fan Yang, and Mingyue Wang. A data-dependent algorithm for querying earth mover’s distance with low doubling dimensions. In *Proceedings of the 2021 SIAM International Conference on Data Mining (SDM)*, pp. 630–638. SIAM, 2021.

- Alexandre Dolgui, Dmitry Ivanov, Suresh P Sethi, and Boris Sokolov. Scheduling in production, supply chain and industry 4.0 systems by optimal control: fundamentals, state-of-the-art and applications. *International journal of production research*, 57(2):411–432, 2019.
- Darko Drakulic, Sofia Michel, Florian Mai, Arnaud Sors, and Jean-Marc Andreoli. BQ-NCO: Bisimulation quotienting for efficient neural combinatorial optimization. In *Thirty-seventh Conference on Neural Information Processing Systems*, 2023. URL <https://openreview.net/forum?id=BRqlkTDvvm>.
- Pavel Dvurechensky, Alexander Gasnikov, and Alexey Kroshnin. Computational optimal transport: Complexity by accelerated gradient descent is better than by sinkhorn’s algorithm. In *International conference on machine learning*, pp. 1367–1376. PMLR, 2018.
- Paul Erdős and Alfréd Rényi. On the evolution of random graphs. *Publ. Math. Inst. Hungar. Acad. Sci*, 5:17–61, 1960.
- Dan Feldman and Michael Langberg. A unified framework for approximating and clustering data. In *Proceedings of the forty-third annual ACM symposium on Theory of computing*, pp. 569–578, 2011.
- Aurélien Froger, Michel Gendreau, Jorge E Mendoza, Éric Pinson, and Louis-Martin Rousseau. Maintenance scheduling in the electricity industry: A literature review. *European Journal of Operational Research*, 251(3):695–706, 2016.
- Zhang-Hua Fu, Kai-Bin Qiu, and Hongyuan Zha. Generalize a small pre-trained model to arbitrarily large tsp instances. In *Proceedings of the AAAI conference on artificial intelligence*, volume 35, pp. 7474–7482, 2021.
- Simon Geisler, Johanna Sommer, Jan Schuchardt, Aleksandar Bojchevski, and Stephan Günnemann. Generalization of neural combinatorial solvers through the lens of adversarial robustness. In *International Conference on Learning Representations*, 2021.
- Teofilo F Gonzalez. Clustering to minimize the maximum intercluster distance. *Theoretical computer science*, 38:293–306, 1985.
- John C Gower and Garnt B Dijkstra. *Procrustes problems*, volume 30. OUP Oxford, 2004.
- Sergey Guminov, Pavel Dvurechensky, and Alexander Gasnikov. On accelerated alternating minimization. 2020.
- Sariel Har-Peled and Soham Mazumdar. On coresets for k-means and k-median clustering. In *Proceedings of the thirty-sixth annual ACM symposium on Theory of computing*, pp. 291–300, 2004.
- Sariel Har-Peled and Manor Mendel. Fast construction of nets in low dimensional metrics, and their applications. In *Proceedings of the twenty-first annual symposium on Computational geometry*, pp. 150–158, 2005.
- Keld Helsgaun. An extension of the lin-kernighan-helsgaun tsp solver for constrained traveling salesman and vehicle routing problems. *Roskilde: Roskilde University*, 12, 2017.
- André Hottung, Bhanu Bhandari, and Kevin Tierney. Learning a latent search space for routing problems using variational autoencoders. In *International Conference on Learning Representations*, 2020.
- Jiawei Huang, Ruomin Huang, Wenjie Liu, Nikolaos Freris, and Hu Ding. A novel sequential coreset method for gradient descent algorithms. In *International Conference on Machine Learning*, pp. 4412–4422. PMLR, 2021.
- Lingxiao Huang, Shaofeng H-C Jiang, Jianing Lou, and Xuan Wu. Near-optimal coresets for robust clustering. In *The Eleventh International Conference on Learning Representations*, 2022.
- Arun Jambulapati, Aaron Sidford, and Kevin Tian. A direct tilde $\{O\}(1/\epsilon)$ iteration parallel algorithm for optimal transport. *Advances in Neural Information Processing Systems*, 32, 2019.

- Chaitanya K. Joshi and Rishabh Anand. Recent advances in deep learning for routing problems. In *ICLR Blog Track*, 2022. URL <https://iclr-blog-track.github.io/2022/03/25/deep-learning-for-routing-problems/>. <https://iclr-blog-track.github.io/2022/03/25/deep-learning-for-routing-problems/>.
- Chaitanya K Joshi, Thomas Laurent, and Xavier Bresson. An efficient graph convolutional network technique for the travelling salesman problem. *arXiv preprint arXiv:1906.01227*, 2019.
- Elias Khalil, Hanjun Dai, Yuyu Zhang, Bistra Dilkina, and Le Song. Learning combinatorial optimization algorithms over graphs. *Advances in neural information processing systems*, 30, 2017.
- Minsu Kim, Jinkyoo Park, et al. Learning collaborative policies to solve np-hard routing problems. *Advances in Neural Information Processing Systems*, 34:10418–10430, 2021.
- Minsu Kim, Junyoung Park, and Jinkyoo Park. Sym-nco: Leveraging symmetry for neural combinatorial optimization. *Advances in Neural Information Processing Systems*, 35:1936–1949, 2022.
- Wouter Kool, Herke van Hoof, and Max Welling. Attention, learn to solve routing problems! In *International Conference on Learning Representations*, 2018.
- Robert Krauthgamer and James R Lee. Navigating nets: simple algorithms for proximity search. In *SODA*, volume 4, pp. 798–807, 2004.
- Yeong-Dae Kwon, Jinho Choo, Byoungjip Kim, Iljoo Yoon, Youngjune Gwon, and Seungjai Min. Pomo: Policy optimization with multiple optima for reinforcement learning. *Advances in Neural Information Processing Systems*, 33:21188–21198, 2020.
- Yeong-Dae Kwon, Jinho Choo, Iljoo Yoon, Minah Park, Duwon Park, and Youngjune Gwon. Matrix encoding networks for neural combinatorial optimization. *Advances in Neural Information Processing Systems*, 34:5138–5149, 2021.
- Sebastian Lamm, Peter Sanders, Christian Schulz, Darren Strash, and Renato F Werneck. Finding near-optimal independent sets at scale. In *2016 Proceedings of the Eighteenth Workshop on Algorithm Engineering and Experiments (ALENEX)*, pp. 138–150. SIAM, 2016.
- A Laterre, Y Fu, MK Jabri, AS Cohen, D Kas, K Hajjar, TS Dahl, A Kerkeni, and K Beguir. Ranked reward: Enabling self-play reinforcement learning for combinatorial optimization. *Advances in Neural Information Processing Systems 31 (NeurIPS 2018)*, 2018.
- Yin Tat Lee and Aaron Sidford. Efficient inverse maintenance and faster algorithms for linear programming. In *2015 IEEE 56th annual symposium on foundations of computer science*, pp. 230–249. IEEE, 2015.
- Yang Li, Jinpei Guo, Runzhong Wang, and Junchi Yan. T2t: From distribution learning in training to gradient search in testing for combinatorial optimization. In *Thirty-seventh Conference on Neural Information Processing Systems*, 2023.
- Zhuwen Li, Qifeng Chen, and Vladlen Koltun. Combinatorial optimization with graph convolutional networks and guided tree search. *Advances in neural information processing systems*, 31, 2018.
- Jian Liang, Ran He, and Tieniu Tan. A comprehensive survey on test-time adaptation under distribution shifts. *arXiv preprint arXiv:2303.15361*, 2023.
- Tianyi Lin, Nhat Ho, and Michael Jordan. On efficient optimal transport: An analysis of greedy and accelerated mirror descent algorithms. In *International Conference on Machine Learning*, pp. 3982–3991. PMLR, 2019.
- Ruiwu Liu, Xiaocen Li, and Kit S Lam. Combinatorial chemistry in drug discovery. *Current opinion in chemical biology*, 38:117–126, 2017.
- Fu Luo, Xi Lin, Fei Liu, Qingfu Zhang, and Zhenkun Wang. Neural combinatorial optimization with heavy decoder: Toward large scale generalization. In *Thirty-seventh Conference on Neural Information Processing Systems*, 2023.

- Konstantin Makarychev, Yury Makarychev, and Ilya Razenshteyn. Performance of johnson–lindenstrauss transform for k-means and k-medians clustering. *SIAM Journal on Computing*, (0):STOC19–269, 2022.
- Fionn Murtagh and Pedro Contreras. Algorithms for hierarchical clustering: an overview. *Wiley Interdisciplinary Reviews: Data Mining and Knowledge Discovery*, 2(1):86–97, 2012.
- Mohammadreza Nazari, Afshin Oroojlooy, Lawrence Snyder, and Martin Takác. Reinforcement learning for solving the vehicle routing problem. *Advances in neural information processing systems*, 31, 2018.
- Gurobi Optimization. Gurobi optimizer reference manual. <https://www.gurobi.com/>, 2020.
- Gabriel Peyré, Marco Cuturi, et al. Computational optimal transport. *Center for Research in Economics and Statistics Working Papers*, (2017-86), 2017.
- Ruizhong Qiu, Zhiqing Sun, and Yiming Yang. Dimes: A differentiable meta solver for combinatorial optimization problems. *Advances in Neural Information Processing Systems*, 35:25531–25546, 2022.
- Gerhard Reinelt. TspLib—a traveling salesman problem library. *ORSA journal on computing*, 3(4):376–384, 1991.
- Frédéric Ros and Serge Guillaume. *Sampling techniques for supervised or unsupervised tasks*. Springer, 2020.
- Shai Shalev-Shwartz and Shai Ben-David. *Understanding machine learning: From theory to algorithms*. Cambridge university press, 2014.
- Yu Sun, Xiaolong Wang, Zhuang Liu, John Miller, Alexei Efros, and Moritz Hardt. Test-time training with self-supervision for generalization under distribution shifts. In *International conference on machine learning*, pp. 9229–9248. PMLR, 2020.
- Zhiqing Sun and Yiming Yang. DIFUSCO: Graph-based diffusion solvers for combinatorial optimization. In *Thirty-seventh Conference on Neural Information Processing Systems*, 2023. URL <https://openreview.net/forum?id=JV8Ff0lgVV>.
- Joshua B Tenenbaum, Vin de Silva, and John C Langford. A global geometric framework for nonlinear dimensionality reduction. *science*, 290(5500):2319–2323, 2000.
- Murad Tukan, Alaa Maalouf, and Dan Feldman. Coresets for near-convex functions. *Advances in Neural Information Processing Systems*, 33:997–1009, 2020.
- Matthew Veres and Medhat Moussa. Deep learning for intelligent transportation systems: A survey of emerging trends. *IEEE Transactions on Intelligent transportation systems*, 21(8):3152–3168, 2019.
- Oriol Vinyals, Meire Fortunato, and Navdeep Jaitly. Pointer networks. *Advances in neural information processing systems*, 28, 2015.
- Zixiu Wang, Yiwen Guo, and Hu Ding. Robust and fully-dynamic coreset for continuous-and-bounded learning (with outliers) problems. *Advances in Neural Information Processing Systems*, 34:14319–14331, 2021.
- Yaoxin Wu, Wen Song, Zhiguang Cao, Jie Zhang, and Andrew Lim. Learning improvement heuristics for solving routing problems. *IEEE transactions on neural networks and learning systems*, 33(9):5057–5069, 2021.
- Liang Xin, Wen Song, Zhiguang Cao, and Jie Zhang. Step-wise deep learning models for solving routing problems. *IEEE Transactions on Industrial Informatics*, 17(7):4861–4871, 2020.
- Liang Xin, Wen Song, Zhiguang Cao, and Jie Zhang. Multi-decoder attention model with embedding glimpse for solving vehicle routing problems. In *Proceedings of the AAAI Conference on Artificial Intelligence*, volume 35, pp. 12042–12049, 2021.

A OTHER PRELIMINARIES

Lemma A.1 (Generalized triangle inequalities Makarychev et al. (2022)). *Given three points a, b, c , the following inequalities hold for any $0 < t \leq 1$:*

- $\text{dist}^2(a, b) \leq (1 + t) \cdot \text{dist}^2(a, c) + (1 + \frac{1}{t}) \cdot \text{dist}^2(b, c)$;
- $|\text{dist}^2(a, c) - \text{dist}^2(b, c)| \leq t \cdot \text{dist}^2(a, c) + \frac{6}{t} \cdot \text{dist}^2(a, b)$.

Definition A.2 (Wasserstein distance (Peyré et al., 2017)). *Let $\mu = \sum_{i=1}^n a_i \delta_{x_i}, \nu = \sum_{j=1}^n b_j \delta_{y_j} \in \mathcal{P}(\mathbb{R}^d)$, where $\mathbf{a}, \mathbf{b} \in \mathbb{R}_+^n$ are their weights and $\{x_i\}_{i \in [n]}, \{y_j\}_{j \in [n]} \subset \mathbb{R}^d$ are their locations. Given a cost matrix $\mathbf{C} \in \mathbb{R}_+^{n \times n}$ with $C_{ij} = \|x_i - y_j\|^2$, the Wasserstein distance between μ and ν is*

$$W(\mu, \nu) := \left(\min_{\mathbf{P} \in \Pi(\mathbf{a}, \mathbf{b})} \langle \mathbf{P}, \mathbf{C} \rangle \right)^{1/2},$$

where $\Pi(\mathbf{a}, \mathbf{b}) := \{\mathbf{P} \in \mathbb{R}_+^{n \times n} \mid \mathbf{P}\mathbf{1} = \mathbf{a}, \mathbf{P}^T\mathbf{1} = \mathbf{b}\}$ is the coupling set and $\mathbf{1}$ is the vector of ones.

A.1 OTHER RELATED WORKS

NCO The existing NCO methods can be categorized into two types: constructive heuristics (Khalil et al., 2017; Kool et al., 2018; Kwon et al., 2020; Hottung et al., 2020; Kim et al., 2022; Joshi et al., 2019; Fu et al., 2021; Geisler et al., 2021; Qiu et al., 2022; Sun & Yang, 2023; Luo et al., 2023; Vinyals et al., 2015; Bello et al., 2016; Nazari et al., 2018; Deudon et al., 2018; Xin et al., 2020; 2021; Kwon et al., 2021; Kim et al., 2021; Cheng et al., 2023; Drakulic et al., 2023) and improvement heuristics (Li et al., 2018; d O Costa et al., 2020; Wu et al., 2021; Chen & Tian, 2019; Li et al., 2023; Chen & Tian, 2019; Hottung et al., 2020; Joshi & Anand, 2022; Joshi et al., 2019) methods; the former can be further divided into two subtypes: autoregressive methods and non-autoregressive methods. The autoregressive methods grow a partial solution to a complete solution incrementally, and the non-autoregressive methods directly predict a heatmap. The improvement heuristic methods often work by iteratively improving a feasible initial solution.

Coreset Coreset is a popular data compression technique for clustering Chen (2009); Feldman & Langberg (2011); Braverman et al. (2022), regression Tukan et al. (2020) and optimization Huang et al. (2022); Wang et al. (2021). More relevant, Huang et al. (2021) proposed a sequential coreset for optimization problems with the Lipschitz smoothness property. Wang et al. (Wang et al., 2021) designed a coreset method for continuous-and-bounded learning (Shalev-Shwartz & Ben-David, 2014). However, these methods cannot offer an efficient method for aligning CO instances with training data in the inference phase.

Optimal transportation (OT) Discrete Wasserstein distance is a special case of OT, thus it can be computed by standard OT solvers. In recent years, a lot of algorithms have been proposed to solve OT problem. For example, interior point method can compute an ϵ_+ -approximation value for OT with $\tilde{O}(n^3)$ time in practice (Peyré et al., 2017) or $\tilde{O}(n^{2.5})$ in theory (Lee & Sidford, 2015). To obtain an ϵ_+ -approximation solution of OT, Sinkhorn algorithm takes $\tilde{O}(n^2/\epsilon_+^2)$ time (Dvurechensky et al., 2018; Lin et al., 2019) by solving the entropic regularization OT (Cuturi, 2013); the accelerated version of Sinkhorn algorithm yields $\tilde{O}(n^{2.5}/\epsilon_+)$ time (Guminov et al., 2020); especially, based on area-convexity and dual extrapolation, Jambulapati et al. (2019) achieved $\tilde{O}(n^2/\epsilon_+)$ time complexity.

B OTHER ALGORITHMS

Algorithm for computing RWD We define two discrete probability measures

$$\alpha = \sum_{i=1}^n a_i \delta_{x_i}, \beta = \sum_{j=1}^n b_j \delta_{y_j} \in \mathcal{P}(\mathbb{R}^d), \quad (6)$$

where $\mathbf{a}, \mathbf{b} \in \mathbb{R}_+^n$ are their weights and $\{x_i\}_{i \in [n]}, \{y_j\}_{j \in [n]} \subseteq \mathbb{R}^d$ their locations; δ is the Dirac delta function. We denote the Wasserstein distance between α and β by $W(\alpha, \beta)$.

The aim of Algorithm 4 is to find a rigid transformation e such that $\mathcal{W}(\alpha, \beta) = W(e \circ \alpha, \beta)$. We initialize $\tilde{\alpha} = \alpha$. We solve $\mathcal{W}(\alpha, \beta)$ by updating the coupling \mathbf{P} and rigid transformation e alternatively. Specifically, we **first** obtain coupling \mathbf{P} by computing $W(\tilde{\alpha}, \beta)$ according to the method in (Jambulapati et al., 2019). **Then**, we fix \mathbf{P} , and compute $\arg \min_e \mathcal{W}_{\mathbf{P}}(e \circ \alpha, \beta)$.

We partition the rigid transformation e into translation transformation e_1 and orthogonal transformation e_2 ; that is, $e = e_2 \circ e_1$. The translation transformation can be updated as $e_1 = \sum_{i=1}^n \sum_{j=1}^n P_{ij} y_j - \sum_{i=1}^n \sum_{j=1}^n P_{ij} x_i$. For fixed e_1, \mathbf{P} , computing the optimal orthogonal transformation e_2 is an orthogonal Procrustes problem (Gower & Dijksterhuis, 2004). More specifically, we first obtain $\mathbf{M} = \sum_{ij} P_{ij} x_i y_j^T$, and apply singular value decomposition $\mathbf{M} = \mathbf{U} \mathbf{D} \mathbf{V}^T$; then, we have

$$e_2 = \mathbf{U} \mathbf{V}^T. \quad (7)$$

Algorithm 3 Algorithm for RWD

Input: α, β

- 1: $t = 0, \tilde{\alpha} = \alpha$;
- 2: **for** $t < T_{align}$ **do**
- 3: $t = t + 1$;
- 4: ▷ **update coupling \mathbf{P}**
Obtain coupling \mathbf{P} by computing $W(\tilde{\alpha}, \beta)$ according to the method in (Jambulapati et al., 2019);
- 5: ▷ **update translation transformation e_1 and orthogonal transformation e_2**
Compute $e_1 = \sum_{i=1}^n \sum_{j=1}^n P_{ij} y_j - \sum_{i=1}^n \sum_{j=1}^n P_{ij} x_i$;
Compute $e_2 = \mathbf{U} \mathbf{V}^T$ according to Equation (7), and set $e = e_2 \circ e_1$;
 $\tilde{\alpha} = \sum_{i=1}^n a_i \delta_{(e \circ x_i)}$.
- 6: **end for**

Output: \mathbf{P}, e

Time complexity of Algorithm 3 We compute the RWD by alternating between optimizing the coupling matrix and the rigid transformation, which is a heuristic method. We assuming that the point dimension d and the number of iterations T_{align} are constants. For computing the coupling matrix, we solve an OT problem within $\tilde{O}(n^2)$ time Jambulapati et al. (2019). The rigid transformation is obtained by solving an orthogonal Procrustes problem, which has a time complexity of $O(n^2 d + n d^2 + d^3)$. Thus, the overall complexity of this heuristic method remains $\tilde{O}(n^2)$.

Algorithm for alignment Here, we introduce our alignment algorithm. We first initialize the current node v as the root node v_0 . Then, we walk from the root node to a leaf node by selecting the most similar measure with the test instance μ .

Algorithm 4 Algorithm for alignment

Input: the tree \mathcal{T} , CO instance μ

- 1: $v = v_0$ ▷ **The current node v is initialized as root node v_0 .**
- 2: Initialize *target* by any measure in coreset \mathcal{S} .
▷ \mathcal{S} is the corresponding coreset maintained in tree \mathcal{T} .
- 3: Select the child v' that is closest to μ under metric RWD.
- 4: Set $v = v'$.
- 5: **if** $\mathcal{W}(\mu, v'.\text{center}) \leq \mathcal{W}(\mu, \text{target})$ **then**
- 6: $\text{target} = v'.\text{center}$;
- 7: **end if**
- 8: If v is not a leaf, jump to Line 4.

Output: *target*

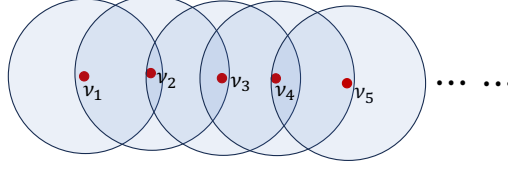


Figure 4: The illustration for error.

C OMITED PROOFS

Proof of Theorem 3.3. The proof sketch is listed here. First, we prove that by taking $(\mathcal{Q}, \text{ddim}, r)$ as input, the coreset constructed by Algorithm 2 can cover the dataset \mathcal{Q} by small balls of radius r by using mathematical induction. Then, we obtain that the value difference of the loss function between the data itself and its representation is small by Lipschitz continuous property. Third, by setting some parameters properly, we turn the additive error into a relative error, and obtain an ϵ -coreset \mathcal{S} .

Given a probability measure $\mu \in \mathcal{Q}$, we assume that its corresponding ball center in the h -th epoch is ν_h .

Claim C.1. $\mathcal{W}^2(\mu, \nu_h) \leq h^2 \cdot \frac{r^2}{H^2}$.

Proof. The error is grown in a manner illustrated in Figure 4. Next, we prove this claim by using mathematical induction.

Base Case: For the case $h = 1$, in the 1-st epoch, we have $\mathcal{W}^2(\mu, \nu_1) \leq \frac{r^2}{H^2}$.

Induction step: For the case $h = m$, in the m -th epoch, we assume that

$$\mathcal{W}^2(\mu, \nu_m) \leq m^2 \cdot \frac{r^2}{H^2}. \quad (8)$$

Then, according to the generalized triangle inequalities in Lemma A.1, we have

$$\mathcal{W}^2(\mu, \nu_{m+1}) \leq (1+t) \cdot \mathcal{W}^2(\mu, \nu_m) + (1+\frac{1}{t}) \cdot \mathcal{W}^2(\nu_m, \nu_{m+1}). \quad (9)$$

Since the radius of small ball in Figure 4 is at most $\frac{r}{H}$, we have $\mathcal{W}^2(\nu_m, \nu_{m+1}) < \frac{r^2}{H^2}$. By using the the induction hypothesis and setting $t = \frac{1}{m}$, we have

$$\mathcal{W}^2(\mu, \nu_{m+1}) \leq (1 + \frac{1}{m}) \cdot m^2 \cdot \frac{r^2}{H^2} + (1+m) \cdot \frac{r^2}{H^2} = (m+1)^2 \frac{r^2}{H^2}. \quad (10)$$

Till now, we prove the case $h = m + 1$. □

Let $\nu := \nu_H$ be the representation of μ in Algorithm 2. According to Claim C.1, we have $\mathcal{W}^2(\mu, \nu) \leq r^2$.

Next, since loss function is L -Lipschitz continuous with respect to RWD on \mathcal{Q} , we have

$$|\ell(\mu, \theta) - \ell(\nu, \theta)| \leq L \cdot \mathcal{W}(\nu, \mu) \leq L \cdot r. \quad (11)$$

$$|\ell(\mathcal{Q}, \theta) - \ell(\mathcal{S}, \theta)| \leq \sum_{\mu \in \mathcal{Q}} w_{\mathcal{Q}}(\mu) \cdot |\ell(\mu, \theta) - \ell(\nu, \theta)| \leq \sum_{\mu \in \mathcal{Q}} w_{\mathcal{Q}}(\mu) \cdot L \cdot r = L \cdot r, \quad (12)$$

where $\nu \in \mathcal{S}$ is the corresponding representation of $\mu \in \mathcal{Q}$, and we have $w_{\mathcal{Q}}(\mathcal{Q}) := \sum_{\mu} w_{\mathcal{Q}}(\mu) = 1$ according to Definition 2.1.

Finally, we have $|\ell(\mathcal{Q}, \theta)| \geq \gamma$, by setting $r = \frac{\epsilon\gamma}{L}$, we obtain the coreset property

$$|\ell(\mathcal{Q}, \theta) - \ell(\mathcal{S}, \theta)| \leq \epsilon\gamma \leq \epsilon \cdot |\ell(\mathcal{Q}, \theta)|. \quad (13)$$

□

D FULL EXPERIMENTS WITH TSP

We take TSP100 as an example to show the advantages of our coreset method. All experiments are conducted on an NVIDIA L20 GPU.

Dataset We apply our method on TSP100-2D/3D Euclidean instances. The labels of TSP100-2D instances are obtained by using the LKH-3 heuristic solver (Helsgaun, 2017); each coordinate of the nodes in a TSP instance is generated by $x\%10$, where x is randomly sampled either from a normal distribution $\mathcal{N}(0, \sigma^2)$ or uniform sampling $\mathcal{U}(0, 10)$. Our training data, TSP100-2D- $\mathcal{N}(0, 1)$ and TSP100-3D- $\mathcal{N}(0, 1)$, consists of 125,000 instances generated by the normal distribution $\mathcal{N}(0, 1)$ and 3000 instances by the uniform distribution $\mathcal{U}(0, 10)$. While the training dataset TSP100-2D- $\mathcal{U}(0, 10)$ consists of 128000 instances generated by uniform distribution $\mathcal{U}(0, 10)$.

Indeed, the distributions of the training dataset TSP100-2D- $\mathcal{N}(0, 1)$ and TSP100-3D- $\mathcal{N}(0, 1)$ are very close to the normal distribution $\mathcal{N}(0, 1)$. Hence, we regard the test data sampled from distribution $\mathcal{N}(0, 1)$ as having no distribution shift. The test data are sampled from a single distribution, either a normal distribution or uniform distribution. Specifically, we sample 1280 test data for TSP100, and 128 test data for other cases. Obviously, the uniform distribution has the highest entropy and thus the highest diversity. For these Gaussian distributions, the larger the variance, the larger the diversity.

As for the TSP100-3D dataset, we can directly extend the 2D instances to 3D instances by appending a third coordinate with a value of zero. Let $X = \{x_i\}_{i \in [n]} \subset \mathbb{R}^3$ are the nodes of an instance. We apply random rotation transformation e on X ; that is, $e(X) := \{e(x_i)\}_{i \in [n]}$. Intuitively, this TSP100-3D dataset has the same intrinsic complexity under metric RWD, which is the low doubling dimension in our assumption.

Table 4: Time statistics for different phases of training on TSP100-2D- $\mathcal{N}(0, 1)$.

Method	Sample size	Labeling time	Coreset Time	Training Time	Total time
Org	128000	4709	-	28563	33272
	4003	147	-	1894	2041
	8245	304	-	2862	3166
US	12951	475	-	4014	4489
	4003	145	691	1731	2567
	8245	305	1086	2747	4138
CS	12951	474	1283	3751	5508

Setting We use the DIFUSCO (Sun & Yang, 2023) as our NCO solver. The model DIFUSCO with Greedy decoding solves TSP instances in an end-to-end manner. We set the learning rate as 0.0002 and the batch size as 64. The diffusion step is performed 50 times in inference phase. We use the cosine schedule described in (Sun & Yang, 2023). To quantify the performance of different methods, we use two criteria: the average tour length (Length) and the total runtime (Time). The term ‘‘Greedy’’ refers to the greedy decoding method of DIFUSCO, and ‘‘2-opt’’ is a post-processing used to improve solutions. The terms US, CS and CS-aligned represent uniform sampling, our coreset without alignment, and our coreset with alignment, respectively. We use the results on the full dataset with 128000 data as a baseline. In experiments, we first construct a coreset \mathcal{S} , and then take $|\mathcal{S}|$ samples by uniform sampling as training datasets.

Results of TSP100-2D Tables 4 to 7 present the results on training dataset TSP100-2D- $\mathcal{N}(0, 1)$. The training datasets are generated by the uniform sampling and our coreset technique respectively. The results show that both our method and uniform sampling method perform better as the sample size increases. Meanwhile, as the sample size decreases, the advantage of our methods compared to uniform sampling becomes increasingly evident.

Moreover, Tables 5 and 6 demonstrate that our method is robust to distribution shift. Specifically, the training data is sampled from a normal distribution $\mathcal{N}(0, 1)$, while the test data is sampled from normal distributions $\mathcal{N}(0, 1)$, $\mathcal{N}(0, 4)$ and a uniform distribution $\mathcal{U}(0, 10)$. The test distributions

Table 5: Comparison of uniform sampling and our coreset method using TSP100-2D- $\mathcal{N}(0, 1)$ as the training dataset on test data TSP100-2D from different distributions.

Sample size	Method	Test distribution	Greedy		Greedy+2-opt	
			Length (\downarrow)	Time (\downarrow)	Length (\downarrow)	Time (\downarrow)
128000	Org	$\mathcal{N}(0, 1)$	20.39	386	18.61	384
		$\mathcal{N}(0, 2)$	42.41	381	37.47	387
		$\mathcal{N}(0, 4)$	76.41	374	67.39	388
		$\mathcal{N}(0, 8)$	87.18	379	77.86	388
		$\mathcal{U}(0, 10)$	89.29	372	79.82	385
4003	US	$\mathcal{N}(0, 1)$	22.34	378	18.92	387
		$\mathcal{N}(0, 2)$	51.59	376	38.25	388
		$\mathcal{N}(0, 4)$	101.95	379	69.28	395
		$\mathcal{N}(0, 8)$	118.83	379	80.38	402
		$\mathcal{U}(0, 10)$	119.78	380	82.59	395
	CS	$\mathcal{N}(0, 1)$	22.21	372	18.87	379
		$\mathcal{N}(0, 2)$	44.94	379	37.80	378
		$\mathcal{N}(0, 4)$	80.63	372	67.92	379
		$\mathcal{N}(0, 8)$	92.63	367	78.47	378
		$\mathcal{U}(0, 10)$	94.73	373	80.64	377
	CS-aligned	$\mathcal{N}(0, 1)$	22.18	359	18.88	363
		$\mathcal{N}(0, 2)$	45.00	357	37.80	362
		$\mathcal{N}(0, 4)$	80.66	362	67.91	358
		$\mathcal{N}(0, 8)$	92.59	362	78.41	358
		$\mathcal{U}(0, 10)$	94.94	361	80.53	360
	US	$\mathcal{N}(0, 1)$	22.12	377	18.87	388
		$\mathcal{N}(0, 2)$	45.59	381	37.86	389
		$\mathcal{N}(0, 4)$	83.17	377	68.13	378
		$\mathcal{N}(0, 8)$	95.16	380	78.81	385
		$\mathcal{U}(0, 10)$	97.31	377	80.80	387
	CS	$\mathcal{N}(0, 1)$	21.79	366	18.84	383
		$\mathcal{N}(0, 2)$	43.72	373	37.73	378
		$\mathcal{N}(0, 4)$	78.72	372	67.79	378
		$\mathcal{N}(0, 8)$	90.44	371	78.36	380
		$\mathcal{U}(0, 10)$	92.99	374	80.35	377
	CS-aligned	$\mathcal{N}(0, 1)$	21.80	360	18.86	359
		$\mathcal{N}(0, 2)$	43.77	354	37.73	356
		$\mathcal{N}(0, 4)$	78.50	361	67.82	358
		$\mathcal{N}(0, 8)$	90.54	350	78.32	359
		$\mathcal{U}(0, 10)$	93.04	355	80.42	361
12951	US	$\mathcal{N}(0, 1)$	21.99	390	18.87	377
		$\mathcal{N}(0, 2)$	44.77	376	37.81	384
		$\mathcal{N}(0, 4)$	80.78	384	67.94	379
		$\mathcal{N}(0, 8)$	93.16	373	78.52	381
		$\mathcal{U}(0, 10)$	95.01	369	80.60	379
	CS	$\mathcal{N}(0, 1)$	21.57	372	18.81	382
		$\mathcal{N}(0, 2)$	43.14	371	37.66	388
		$\mathcal{N}(0, 4)$	77.80	369	67.58	379
		$\mathcal{N}(0, 8)$	89.63	371	78.18	408
		$\mathcal{U}(0, 10)$	92.01	378	80.23	375
	CS-aligned	$\mathcal{N}(0, 1)$	21.50	361	18.79	358
		$\mathcal{N}(0, 2)$	43.18	361	37.66	364
		$\mathcal{N}(0, 4)$	77.67	362	67.57	357
		$\mathcal{N}(0, 8)$	89.60	357	78.18	361
		$\mathcal{U}(0, 10)$	92.01	358	80.21	359

$\mathcal{N}(0, 4)$ and $\mathcal{U}(0, 10)$ are significantly different from the training distribution $\mathcal{N}(0, 1)$, which represent substantial distribution shifts. The results in Tables 5 and 6 show that our method consistently outperforms the baselines, demonstrating its robustness to distribution shifts.

Furthermore, Table 6 shows that models trained on our coreset can generalize better to larger problem sizes such as TSP200, TSP500 and TSP1000. Moreover, Table 7 confirms that our method outperforms other approaches on the TSPLIB dataset. Table 4 shows the time efficiency of our coreset method.

Table 6: Comparison of uniform sampling and our coreset method using TSP100-2D- $\mathcal{N}(0, 1)$ as the training dataset on test data of varying sizes. We fix the sample size as 12951.

TSP size	Method	Test distribution	Greedy		Greedy+2-opt	
			Length (\downarrow)	Time (\downarrow)	Length (\downarrow)	Time (\downarrow)
TSP-200	Org	$\mathcal{N}(0, 1)$	29.85	107	26.61	111
		$\mathcal{N}(0, 2)$	60.87	109	53.38	110
		$\mathcal{N}(0, 4)$	109.70	110	94.90	111
		$\mathcal{N}(0, 8)$	123.39	110	108.41	110
		$\mathcal{U}(0, 10)$	126.99	107	111.50	111
TSP-500	Org	$\mathcal{N}(0, 1)$	50.55	1012	42.38	1018
		$\mathcal{N}(0, 2)$	102.65	1012	84.89	1018
		$\mathcal{N}(0, 4)$	184.40	1012	150.47	1018
		$\mathcal{N}(0, 8)$	204.53	1010	171.14	1014
		$\mathcal{U}(0, 10)$	210.70	1012	175.41	1016
TSP-1000	Org	$\mathcal{N}(0, 1)$	77.15	2826	60.56	2840
		$\mathcal{N}(0, 2)$	157.12	2826	121.45	2839
		$\mathcal{N}(0, 4)$	281.64	4224	214.55	2833
		$\mathcal{N}(0, 8)$	310.94	4218	243.77	4242
		$\mathcal{U}(0, 10)$	317.55	4218	249.28	4236
TSP-200	US	$\mathcal{N}(0, 1)$	33.69	109	27.14	112
		$\mathcal{N}(0, 2)$	69.77	109	54.28	112
		$\mathcal{N}(0, 4)$	125.99	108	96.70	112
		$\mathcal{N}(0, 8)$	143.76	109	110.64	113
		$\mathcal{U}(0, 10)$	145.41	109	113.39	112
	CS	$\mathcal{N}(0, 1)$	30.75	107	26.69	110
		$\mathcal{N}(0, 2)$	62.08	109	53.36	112
		$\mathcal{N}(0, 4)$	110.48	109	94.84	111
		$\mathcal{N}(0, 8)$	127.06	107	108.76	111
		$\mathcal{U}(0, 10)$	129.77	107	111.47	109
	CS-aligned	$\mathcal{N}(0, 1)$	30.77	77	26.68	79
		$\mathcal{N}(0, 2)$	61.87	76	53.38	79
		$\mathcal{N}(0, 4)$	110.99	78	94.59	79
		$\mathcal{N}(0, 8)$	126.69	76	108.42	79
		$\mathcal{U}(0, 10)$	129.28	76	111.4	9 78
	US	$\mathcal{N}(0, 1)$	59.81	1012	43.41	1020
		$\mathcal{N}(0, 2)$	126.00	1013	86.76	1022
		$\mathcal{N}(0, 4)$	237.72	1012	154.28	1022
		$\mathcal{N}(0, 8)$	261.79	1013	176.13	1022
		$\mathcal{U}(0, 10)$	263.66	1015	180.75	1022
	CS	$\mathcal{N}(0, 1)$	49.11	1012	42.25	1016
		$\mathcal{N}(0, 2)$	99.58	1012	84.60	1019
		$\mathcal{N}(0, 4)$	178.56	1010	149.50	1016
		$\mathcal{N}(0, 8)$	205.86	1012	170.54	1016
		$\mathcal{U}(0, 10)$	208.36	1011	174.93	1016
	CS-aligned	$\mathcal{N}(0, 1)$	49.38	680	42.26	683
		$\mathcal{N}(0, 2)$	99.66	680	84.52	684
		$\mathcal{N}(0, 4)$	178.88	679	149.63	682

Continued on next page

– continued from previous page

TSP size	Method	Test distribution	Greedy		Greedy+2-opt	
			Length (\downarrow)	Time (\downarrow)	Length (\downarrow)	Time (\downarrow)
TSP-1000	US	$\mathcal{N}(0, 8)$	204.42	678	170.62	682
		$\mathcal{U}(0, 10)$	208.77	678	175.03	682
		$\mathcal{N}(0, 1)$	94.71	2823	61.72	2848
		$\mathcal{N}(0, 2)$	199.22	2825	123.56	2849
		$\mathcal{N}(0, 4)$	382.77	4224	219.16	2847
		$\mathcal{N}(0, 8)$	421.29	4218	249.08	4258
		$\mathcal{U}(0, 10)$	426.61	4215	255.95	4254
		$\mathcal{N}(0, 1)$	69.76	2823	59.59	2833
		$\mathcal{N}(0, 2)$	141.06	2825	119.64	2832
		$\mathcal{N}(0, 4)$	252.92	4224	210.71	2832
	CS	$\mathcal{N}(0, 8)$	293.49	4218	240.42	4236
		$\mathcal{U}(0, 10)$	299.80	4215	246.57	4234
		$\mathcal{N}(0, 1)$	69.96	2825	59.57	2832
		$\mathcal{N}(0, 2)$	140.95	2822	119.39	2833
		$\mathcal{N}(0, 4)$	253.63	2821	210.81	2830
	CS-aligned	$\mathcal{N}(0, 8)$	293.82	2815	240.11	2826
		$\mathcal{U}(0, 10)$	300.03	2812	246.61	2827

Table 7: Comparison of uniform sampling and our coreset method using TSP100-2D- $\mathcal{N}(0, 1)$ as the training dataset on test data TSPLIB(Reinelt, 1991).

Sample size	Method	Test distribution	Greedy		Greedy+2-opt	
			Length (\downarrow)	Time (\downarrow)	Length (\downarrow)	Time (\downarrow)
128000	Org	$\mathcal{N}(0, 1)$	129.35	108	112.23	106
4003	US	$\mathcal{N}(0, 1)$	190.79	109	115.87	108
	CS	$\mathcal{N}(0, 1)$	153.08	107	113.56	108
	CS-aligned	$\mathcal{N}(0, 1)$	152.70	103	113.71	105
8245	US	$\mathcal{N}(0, 1)$	166.40	106	114.47	108
	CS	$\mathcal{N}(0, 1)$	140.49	107	113.04	106
	CS-aligned	$\mathcal{N}(0, 1)$	140.18	104	112.91	104
12951	US	$\mathcal{N}(0, 1)$	162.19	107	114.31	107
	CS	$\mathcal{N}(0, 1)$	133.63	106	112.45	105
	CS-aligned	$\mathcal{N}(0, 1)$	133.14	103	112.52	110

Results of TSP100-3D- $\mathcal{N}(0, 1)$ Tables 8 to 10 show the results of TSP100-3D- $\mathcal{N}(0, 1)$. Table 8 illustrates the overall acceleration improvement. For the test data without distribution shift, our method has comparable performance; for the test data occurring distribution shift, our method has better performance. Moreover, our coreset with alignment version performs better in the TSP-3D case. From Tables 9 and 10, alignment can perform better for higher dimension dataset (i.e., TSP-3D). Thus, the alignment version is promising for tackling high-dimensional data.

Table 8: Time statistics for different phases of training on TSP100-3D- $\mathcal{N}(0, 1)$.

Method	Sample size	Labeling time	Coreset Time	Training Time	Total time
Org	128000	4940	-	30671	35611
US	4103	160	-	2102	2262
	7960	307	-	2729	3036
	12058	466	-	3514	3980
	4103	159	1012	2080	1379
CS	7960	309	1177	2712	4198
	12058	463	1675	3493	5631

Table 9: Comparison of uniform sampling and our coreset method using TSP100-3D- $\mathcal{N}(0, 1)$ as the training dataset on test data TSP100-3D from different distributions.

Sample size	Method	Test distribution	Greedy Length (\downarrow)	Greedy Time (\downarrow)	Alignment time (\downarrow)
128000	Org	$\mathcal{N}(0, 1)$	20.80	364	-
		$\mathcal{N}(0, 2)$	42.25	366	-
		$\mathcal{N}(0, 4)$	76.57	362	-
		$\mathcal{N}(0, 8)$	88.45	360	-
		$\mathcal{U}(0, 10)$	90.55	358	-
	US	$\mathcal{N}(0, 1)$	24.92	480	-
		$\mathcal{N}(0, 2)$	49.96	482	-
		$\mathcal{N}(0, 4)$	96.60	483	-
		$\mathcal{N}(0, 8)$	116.65	482	-
		$\mathcal{U}(0, 10)$	119.78	481	-
4103	CS	$\mathcal{N}(0, 1)$	24.89	364	-
		$\mathcal{N}(0, 2)$	50.46	384	-
		$\mathcal{N}(0, 4)$	106.35	360	-
		$\mathcal{N}(0, 8)$	109.12	360	-
		$\mathcal{U}(0, 10)$	111.63	353	-
	CS-aligned	$\mathcal{N}(0, 1)$	23.36	479	2
		$\mathcal{N}(0, 2)$	47.00	480	4
		$\mathcal{N}(0, 4)$	91.94	479	7
		$\mathcal{N}(0, 8)$	106.50	482	9
		$\mathcal{U}(0, 10)$	108.81	483	11
	US	$\mathcal{N}(0, 1)$	23.62	477	-
		$\mathcal{N}(0, 2)$	48.32	477	-
		$\mathcal{N}(0, 4)$	92.92	484	-
		$\mathcal{N}(0, 8)$	111.98	479	-
		$\mathcal{U}(0, 10)$	115.62	481	-
7960	CS	$\mathcal{N}(0, 1)$	23.41	362	-
		$\mathcal{N}(0, 2)$	47.10	361	-
		$\mathcal{N}(0, 4)$	86.20	362	-
		$\mathcal{N}(0, 8)$	99.50	365	-
		$\mathcal{U}(0, 10)$	101.25	359	-
	CS-aligned	$\mathcal{N}(0, 1)$	22.83	476	12
		$\mathcal{N}(0, 2)$	46.06	474	14
		$\mathcal{N}(0, 4)$	85.71	483	16
		$\mathcal{N}(0, 8)$	97.61	480	17
		$\mathcal{U}(0, 10)$	99.10	481	19
	US	$\mathcal{N}(0, 1)$	22.10	360	-
		$\mathcal{N}(0, 2)$	45.52	368	-
		$\mathcal{N}(0, 4)$	84.28	368	-
		$\mathcal{N}(0, 8)$	98.57	372	-
		$\mathcal{U}(0, 10)$	100.40	367	-
12058	CS	$\mathcal{N}(0, 1)$	22.10	371	-
		$\mathcal{N}(0, 2)$	44.40	362	-
		$\mathcal{N}(0, 4)$	80.47	361	-
		$\mathcal{N}(0, 8)$	93.00	361	-
		$\mathcal{U}(0, 10)$	95.25	362	-
	CS-aligned	$\mathcal{N}(0, 1)$	22.30	396	21
		$\mathcal{N}(0, 2)$	44.80	371	22
		$\mathcal{N}(0, 4)$	79.96	388	23
		$\mathcal{N}(0, 8)$	92.28	377	25
		$\mathcal{U}(0, 10)$	94.13	366	26

Table 10: Comparison of uniform sampling and our coreset method with training dataset TSP100-3D- $\mathcal{N}(0, 1)$ on test data of varying sizes. We fix the sample size as 12058.

TSP size	Method	Test distribution	Greedy		Alignment time (\downarrow)
			Length (\downarrow)	Time (\downarrow)	
TSP-200	Org	$\mathcal{N}(0, 1)$	30.02	77	-
		$\mathcal{N}(0, 2)$	61.03	76	-
		$\mathcal{N}(0, 4)$	109.78	77	-
		$\mathcal{N}(0, 8)$	126.15	76	-
		$\mathcal{U}(0, 10)$	128.35	77	-
TSP-500	Org	$\mathcal{N}(0, 1)$	48.66	682	-
		$\mathcal{N}(0, 2)$	101.71	682	-
		$\mathcal{N}(0, 4)$	184.94	682	-
		$\mathcal{N}(0, 8)$	210.36	680	-
		$\mathcal{U}(0, 10)$	212.62	683	-
TSP-1000	Org	$\mathcal{N}(0, 1)$	69.08	2828	-
		$\mathcal{N}(0, 2)$	144.10	2826	-
		$\mathcal{N}(0, 4)$	264.58	2824	-
		$\mathcal{N}(0, 8)$	303.02	2821	-
		$\mathcal{U}(0, 10)$	313.23	2818	-
TSP-200	US	$\mathcal{N}(0, 1)$	32.30	76	-
		$\mathcal{N}(0, 2)$	67.81	77	-
		$\mathcal{N}(0, 4)$	130.76	77	-
		$\mathcal{N}(0, 8)$	152.74	77	-
		$\mathcal{U}(0, 10)$	153.90	77	-
	CS	$\mathcal{N}(0, 1)$	32.72	76	-
		$\mathcal{N}(0, 2)$	66.08	76	-
		$\mathcal{N}(0, 4)$	120.64	78	-
		$\mathcal{N}(0, 8)$	139.91	77	-
		$\mathcal{U}(0, 10)$	142.84	77	-
	CS-aligned	$\mathcal{N}(0, 1)$	33.25	76	2
		$\mathcal{N}(0, 2)$	69.79	75	5
		$\mathcal{N}(0, 4)$	118.44	77	7
		$\mathcal{N}(0, 8)$	135.90	77	10
		$\mathcal{U}(0, 10)$	138.27	76	12
	US	$\mathcal{N}(0, 1)$	58.45	682	-
		$\mathcal{N}(0, 2)$	127.53	681	-
		$\mathcal{N}(0, 4)$	264.93	682	-
		$\mathcal{N}(0, 8)$	316.73	681	-
		$\mathcal{U}(0, 10)$	318.39	680	-
	CS	$\mathcal{N}(0, 1)$	59.69	682	-
		$\mathcal{N}(0, 2)$	122.24	681	-
		$\mathcal{N}(0, 4)$	231.96	682	-
		$\mathcal{N}(0, 8)$	266.08	677	-
		$\mathcal{U}(0, 10)$	268.75	680	-
	CS-aligned	$\mathcal{N}(0, 1)$	56.47	682	16
		$\mathcal{N}(0, 2)$	121.33	681	19
		$\mathcal{N}(0, 4)$	205.45	682	23
		$\mathcal{N}(0, 8)$	238.14	681	26
		$\mathcal{U}(0, 10)$	245.01	681	30
TSP-500	US	$\mathcal{N}(0, 1)$	86.01	2828	-
		$\mathcal{N}(0, 2)$	191.39	2828	-
		$\mathcal{N}(0, 4)$	397.40	2825	-
		$\mathcal{N}(0, 8)$	470.55	2820	-
		$\mathcal{U}(0, 10)$	550.11	2819	-

Continued on next page

TSP-1000

– continued from previous page

TSP size	Method	Test distribution	Greedy		
			Length (\downarrow)	Time (\downarrow)	
	CS	$\mathcal{N}(0, 1)$	86.57	2826	-
		$\mathcal{N}(0, 2)$	181.84	2827	-
		$\mathcal{N}(0, 4)$	342.64	2822	-
		$\mathcal{N}(0, 8)$	395.66	2820	-
		$\mathcal{U}(0, 10)$	441.82	2818	-
	CS-aligned	$\mathcal{N}(0, 1)$	86.87	2828	236
		$\mathcal{N}(0, 2)$	186.88	2823	433
		$\mathcal{N}(0, 4)$	320.68	2825	624
		$\mathcal{N}(0, 8)$	372.34	2820	861
		$\mathcal{U}(0, 10)$	383.92	2819	980

Then, we take TSP-3D as an example to compare the performance of the random heuristic alignment method (CS-rand-aligned) with our proposed alignment method (CS-aligned).

As shown in Table 11, the results demonstrate that the CS-rand-aligned method performs similarly to the unaligned approach, providing little improvement. In contrast, our alignment method significantly enhances performance, confirming its practical effectiveness.

Table 11: Comparison of rand alignment (CS-rand-aligned) and our alignment (CS-aligned) method with training dataset TSP100-3D- $\mathcal{N}(0, 1)$ on test data of varying sizes. We fix the sample size as 12058.

TSP size	Method	Test distribution	Greedy		Alignment time (\downarrow)
			Length (\downarrow)	Time (\downarrow)	
TSP-100	US	$\mathcal{U}(0, 10)$	100.41	37	-
	CS	$\mathcal{U}(0, 10)$	95.27	36	-
	CS-aligned	$\mathcal{U}(0, 10)$	94.13	37	3
	CS-rand-aligned	$\mathcal{U}(0, 10)$	95.62	37	11
TSP-200	US	$\mathcal{U}(0, 10)$	153.90	77	-
	CS	$\mathcal{U}(0, 10)$	142.84	77	-
	CS-aligned	$\mathcal{U}(0, 10)$	138.27	76	12
	CS-rand-aligned	$\mathcal{U}(0, 10)$	144.84	75	17
TSP-500	US	$\mathcal{U}(0, 10)$	318.39	680	-
	CS	$\mathcal{U}(0, 10)$	268.75	680	-
	CS-aligned	$\mathcal{U}(0, 10)$	245.01	681	30
	CS-rand-aligned	$\mathcal{U}(0, 10)$	255.92	674	23
TSP-1000	US	$\mathcal{U}(0, 10)$	550.11	2819	-
	CS	$\mathcal{U}(0, 10)$	441.82	2826	-
	CS-aligned	$\mathcal{U}(0, 10)$	383.92	2818	980
	CS-rand-aligned	$\mathcal{U}(0, 10)$	429.90	2817	493

Results of TSP100-2D- $\mathcal{U}(0, 10)$ Tables 12 to 15 present the results on training dataset TSP100-2D- $\mathcal{U}(0, 10)$. The training datasets are generated by the uniform sampling and our coresot technique respectively. Table 12 clearly demonstrates the overall acceleration improvement. All the results show that both our method and uniform sampling method perform better as the sample size increases. For both the test data with distribution shift and without distribution shift, our method consistently shows better performance. Table 14 further illustrates that our method can generalize to large-scale TSP problems better. Table 15 confirms that our method outperforms other approaches on the TSPLIB dataset.

Results of TSP100-3D- $\mathcal{U}(0, 10)$ Tables 16 and 17 present the results on training dataset TSP100-2D- $\mathcal{U}(0, 10)$.

Table 12: Time statistics for different phases of training on TSP100-2D- $\mathcal{U}(0, 10)$.

Method	Sample size	Labeling time	Coreset Time	Training Time	Total time
Org	128000	4883	-	27686	32569
US	4003	153	-	2387	2540
	8245	315	-	3217	3532
	12951	495	-	3578	4073
CS	4003	154	859	2331	3344
	8245	315	841	3217	4373
	12951	493	1293	3516	5302

Table 13: Comparison of uniform sampling and our coreset method using TSP100-2D- $\mathcal{U}(0, 10)$ as the training dataset on test data TSP100-2D from different distributions.

Sample size	Method	Test distribution	Greedy		Greedy+2-opt	
			Length (\downarrow)	Time (\downarrow)	Length (\downarrow)	Time (\downarrow)
128000	Org	$\mathcal{U}(0, 10)$	86.77	358	79.53	353
4003	US	$\mathcal{U}(0, 10)$	100.62	355	80.97	375
	CS	$\mathcal{U}(0, 10)$	97.69	461	80.94	383
	CS-aligned	$\mathcal{U}(0, 10)$	97.71	363	80.95	369
	US	$\mathcal{U}(0, 10)$	92.66	352	80.33	365
8245	CS	$\mathcal{U}(0, 10)$	93.12	381	80.38	372
	CS-aligned	$\mathcal{U}(0, 10)$	93.27	351	80.41	354
	US	$\mathcal{U}(0, 10)$	91.98	362	80.34	367
12951	CS	$\mathcal{U}(0, 10)$	92.33	354	80.23	356
	CS-aligned	$\mathcal{U}(0, 10)$	92.39	360	80.28	367

Table 14: Comparison of uniform sampling and our coreset method using TSP100-2D- $\mathcal{U}(0, 10)$ as the training dataset on test data of varying sizes. We fix the sample size as 12951.

TSP size	Method	Test distribution	Greedy		Greedy+2-opt	
			Length (\downarrow)	Time (\downarrow)	Length (\downarrow)	Time (\downarrow)
TSP-200	Org	$\mathcal{U}(0, 10)$	125.06	72	110.89	73
TSP-500	Org	$\mathcal{U}(0, 10)$	195.68	675	172.19	677
TSP-1000	Org	$\mathcal{U}(0, 10)$	276.69	2815	241.59	2824
TSP-200	US	$\mathcal{U}(0, 10)$	130.05	76	111.71	81
	CS	$\mathcal{U}(0, 10)$	129.52	75	111.31	81
	CS-aligned	$\mathcal{U}(0, 10)$	129.95	77	111.35	76
TSP-500	US	$\mathcal{U}(0, 10)$	238.46	677	177.30	682
	CS	$\mathcal{U}(0, 10)$	221.76	677	175.94	682
	CS-aligned	$\mathcal{U}(0, 10)$	221.72	675	175.89	683
TSP-1000	US	$\mathcal{U}(0, 10)$	434.16	2811	254.37	2837
	CS	$\mathcal{U}(0, 10)$	346.71	2811	251.40	2831
	CS-aligned	$\mathcal{U}(0, 10)$	347.46	2813	251.35	2833

Table 15: Comparison of uniform sampling and our coreset method using TSP100-2D- $\mathcal{U}(0, 10)$ as the training dataset on test data TSPLIB(Reinelt, 1991).

Sample size	Method	Test distribution	Greedy		Greedy+2-opt	
			Length (\downarrow)	Time (\downarrow)	Length (\downarrow)	Time (\downarrow)
128000	Org	$\mathcal{N}(0, 1)$	125.39	102	110.90	104
4003	US	$\mathcal{U}(0, 10)$	183.71	104	115.21	110
	CS	$\mathcal{U}(0, 10)$	164.81	106	114.50	108
	CS-aligned	$\mathcal{U}(0, 10)$	166.04	105	114.41	103
	US	$\mathcal{U}(0, 10)$	161.75	107	113.69	107
8245	CS	$\mathcal{U}(0, 10)$	132.06	103	111.52	111
	CS-aligned	$\mathcal{U}(0, 10)$	145.90	103	112.86	103
	US	$\mathcal{U}(0, 10)$	157.10	104	113.98	105
12951	CS	$\mathcal{U}(0, 10)$	140.97	104	112.96	106
	CS-aligned	$\mathcal{U}(0, 10)$	141.81	501	112.81	110

Table 16: Comparison of uniform sampling and our coreset method using TSP100-3D- $\mathcal{U}(0, 10)$ as the training dataset on test data TSP100-3D from different distributions.

Sample size	Method	Test distribution	Greedy	
			Length (\downarrow)	Time (\downarrow)
128000	Org	$\mathcal{U}(0, 10)$	87.84	350
4122	US	$\mathcal{U}(0, 10)$	108.74	350
	CS	$\mathcal{U}(0, 10)$	108.45	352
	CS-aligned	$\mathcal{U}(0, 10)$	106.11	381
	US	$\mathcal{U}(0, 10)$	95.78	360
8245	CS	$\mathcal{U}(0, 10)$	98.53	347
	CS-aligned	$\mathcal{U}(0, 10)$	97.89	358
	US	$\mathcal{U}(0, 10)$	93.38	364
12951	CS	$\mathcal{U}(0, 10)$	93.15	348
	CS-aligned	$\mathcal{U}(0, 10)$	92.91	354

Table 17: Comparison of uniform sampling and our coreset method using TSP100-3D- $\mathcal{U}(0, 10)$ as the training dataset on test data of varying sizes. We fix the sample size as 12951.

TSP size	Method	Test distribution	Greedy	
			Length (\downarrow)	Time (\downarrow)
TSP-200	Org	$\mathcal{U}(0, 10)$	125.98	73
TSP-500	Org	$\mathcal{U}(0, 10)$	210.15	674
TSP-1000	Org	$\mathcal{U}(0, 10)$	313.00	2818
TSP-200	US	$\mathcal{U}(0, 10)$	145.67	78
	CS	$\mathcal{U}(0, 10)$	144.27	76
	CS-aligned	$\mathcal{U}(0, 10)$	143.46	75
TSP-500	US	$\mathcal{U}(0, 10)$	302.16	674
	CS	$\mathcal{U}(0, 10)$	244.63	676
	CS-aligned	$\mathcal{U}(0, 10)$	236.33	689
TSP-1000	US	$\mathcal{U}(0, 10)$	535.90	2815
	CS	$\mathcal{U}(0, 10)$	367.04	2812
	CS-aligned	$\mathcal{U}(0, 10)$	308.71	2816

E FULL EXPERIMENTS WITH MIS

Dataset For Maximal Independent Set (MIS), we train our model on ER-[90-100] dataset (Erdős & Rényi, 1960), where ER-[n - N] means that the graph contains n to N nodes. We set the connection probability as 0.15 as in (Sun & Yang, 2023). The labels of our MIS datasets are obtained by using the KaMIS2 solver. Our training dataset of MIS consists of 128000 ER-[90-100] instances. We evaluate our method on ER-[90-100], ER-[400-500], ER-[900-1000] and SATLIB.

Setting We use the DIFUSCO (Sun & Yang, 2023) as our NCO solver. To quantify the performance of different methods, we use two criteria: the average tour length (Length) and the total runtime (Time). The term “Greedy” refers to the greedy decoding method of DIFUSCO, and “Sampling” is the sampling decoding. The terms US and CS represent uniform sampling and our coresets method, respectively. We use the results on the full dataset with 128000 data as a baseline.

Table 18: Time statistics for different phases of MIS.

Method	Sample size	Labeling time	Coreset Time	Training Time	Total time
Org	128000	102600	-	16762	119362
US	3973	3184	-	1726	4910
	8001	6413	-	2503	8916
	12417	9953	-	3400	13353
	3973	4007	2263	3227	9497
CS	8001	7322	2424	5031	14777
	12417	11032	2511	7011	20554

Table 19: Comparison of uniform sampling and our coresets method with training dataset ER-[90-100] on test data from different distributions.

Sample size	Method	Test distribution	Greedy		Sampling	
			Length (\downarrow)	Time (\downarrow)	Length (\downarrow)	Time (\downarrow)
128000	Org	ER-[v90-100]	22.34	64	23.27	70
		ER-[400-500]	34.66	134	36.69	551
		ER-[700-800]	37.51	393	40.06	1463
3973	US	ER-[v90-100]	19.57	64	21.34	319
		ER-[400-500]	27.84	134	29.48	552
		ER-[700-800]	30.30	391	32.23	1469
	CS	ER-[v90-100]	19.77	63	21.49	72
		ER-[400-500]	27.99	135	29.85	558
		ER-[700-800]	30.61	392	32.38	1524
8001	US	ER-[v90-100]	20.38	64	22.33	70
		ER-[400-500]	28.81	135	30.59	554
		ER-[700-800]	31.28	393	32.77	1471
	CS	ER-[v90-100]	20.25	64	22.27	73
		ER-[400-500]	29.59	134	31.91	549
		ER-[700-800]	32.23	393	33.93	1460
12417	US	ER-[v90-100]	20.80	63	22.30	71
		ER-[400-500]	30.36	135	32.55	549
		ER-[700-800]	32.30	393	34.25	1458
	CS	ER-[v90-100]	21.04	63	22.55	70
		ER-[400-500]	31.00	135	33.11	548
		ER-[700-800]	32.96	393	35.59	1462

Results of MIS Tables 18 to 20 present the results on training dataset ER-[90-100]. The training datasets are generated by the uniform sampling and our coresets technique respectively. Table 18 clearly demonstrates the overall acceleration improvement. All the results show that both our method and uniform sampling method perform better as the sample size increases. Table 19 demonstrates

that our method can generalize to large-scale ER problems better. Table 20 show that the performance of our method and uniform sampling method is similar on SATLIB.

Table 20: Comparison of uniform sampling and our coreset method with training dataset ER-[90-100] on test data SATLIB.

Sample size	Method	Test distribution	Greedy		Sampling	
			Length (\downarrow)	Time (\downarrow)	Length (\downarrow)	Time (\downarrow)
128000	Org	ER-[v90-100]	22.34	64	23.27	70
3973	US	SATLIB	1015.64	120	1022.81	490
	CS	SATLIB	1015.31	122	1021.24	518
8245	US	SATLIB	410.61	296	413.49	898
	CS	SATLIB	409.87	299	413.34	902
12417	US	SATLIB	410.32	304	413.55	906
	CS	SATLIB	410.83	297	414.04	900

F FULL EXPERIMENTS WITH CVRP

Dataset For Capacitated Vehicle Routing Problem (CVRP), we follow the experimental setting in Luo et al. (2023).

Table 21: Comparison of uniform sampling and our coreset method with training dataset CVRP100- $\mathcal{N}(0, 0.1)$ on test data from different distributions.

Sample size	Method	Test distribution	RRC-budget (\downarrow)	Length (\downarrow)	Gap (\downarrow)	Time (\downarrow)
128000	Org	CVRP100	0	17.64	6.34%	3
			50	16.58	-0.02%	45
			100	16.43	-0.96%	86
			200	16.30	-1.70%	162
			500	16.18	-2.43%	397
4437	US	CVRP100	0	19.56	17.91%	3
			50	17.85	7.64%	45
			100	17.57	5.96%	86
			200	17.30	4.28%	162
			500	17.03	2.71%	397
	CS	CVRP100	0	19.16	15.51%	3
			50	17.65	6.41%	45
			100	17.38	4.78%	86
			200	17.15	3.38%	163
			500	16.91	2.01%	400
8082	US	CVRP100	0	18.77	13.18%	3
			50	17.35	4.62%	47
			100	17.13	3.27%	91
			200	16.92	2.01%	172
			500	16.71	0.75%	423
	CS	CVRP100	0	18.49	11.51%	3
			50	17.19	3.66%	45
			100	16.98	2.38%	88
			200	16.78	1.19%	168
			500	16.60	0.06%	413
	US	CVRP100	0	18.65	12.47%	3
			50	17.24	3.95%	47
			100	17.01	2.59%	90
			200	16.82	1.43%	170
			500	16.63	0.25%	415
	CS	CVRP100	0	18.53	11.72%	3
			50	17.18	3.56%	47
			100	16.96	2.23%	90
			200	16.77	1.13%	170
			500	16.58	-0.01%	415

Table 22: Comparison of uniform sampling and our coreset method with training dataset CVRP100- $\mathcal{N}(0, 0.1)$ on test data of varying sizes. We fix the sample size as 12175.

Sample size	Method	Test distribution	RRC-budget (\downarrow)	Length (\downarrow)	Gap (\downarrow)	Time (\downarrow)
128000	Org	CVRP200	0	22.70	12.52%	2
			50	21.50	6.60%	26
			100	21.34	5.77%	49
			200	21.16	4.90%	105
			500	20.96	3.88%	256
		CVRP500	0	41.68	11.95%	2
			50	40.23	8.06%	179
			100	39.91	7.20%	298
			200	39.64	6.48%	604
			500	39.32	5.62%	1628
		CVRP1000	0	44.62	20.29%	73
			50	42.74	15.25%	895
			100	42.36	14.22%	1810
			200	41.81	12.72%	3672
			500	41.19	11.04%	9108
12175	US	CVRP200	0	24.17	19.80 %	2
			50	22.79	12.97%	26
			100	22.52	11.61%	50
			200	22.24	10.27%	108
			500	21.89	8.52%	263
		CVRP200	0	24.00	18.97%	2
			50	22.60	12.03%	25
			100	22.36	10.83%	48
			200	22.13	9.71%	105
			500	21.75	7.84%	256
		CVRP500	0	45.23	21.50%	2
			50	43.40	16.58%	173
			100	42.84	15.06%	288
			200	42.39	13.85%	584
			500	41.82	12.32%	1579
		CVRP500	0	45.10	21.15%	2
			50	43.19	16.00%	173
			100	42.73	14.78%	287
			200	42.28	13.56%	583
			500	41.64	11.85%	1576
12175	US	CVRP1000	0	53.01	42.91%	74
			50	49.42	33.23%	897
			100	48.81	31.60%	1819
			200	47.95	29.28%	3708
			500	46.91	26.48%	9180
		CVRP1000	0	51.88	39.88%	73
			50	48.24	30.06%	892
			100	47.71	28.64%	1805
			200	47.00	26.71%	3672
			500	46.12	24.34%	9108

Table 23: Comparison of uniform sampling and our coreset method with training dataset CVRP100- $\mathcal{N}(0, 0.1)$ on test data CVRPLib.

Sample size	Method	Test distribution	RRC-budget (\downarrow)	Length (\downarrow)	Gap (\downarrow)	Time (\downarrow)
128000	Org	CVRPLib	0	913.17	16.48%	1
			50	787.20	0.41%	4
			100	787.20	0.41%	7
			200	787.20	0.41%	12
			500	787.20	0.41%	29
4437	US	CVRPLib	0	927.95	18.36%	1
			50	868.66	10.80%	4
			100	864.51	10.27%	7
			200	844.59	7.73%	14
			500	844.59	7.73%	33
	CS	CVRPLib	0	950.06	21.18%	1
			50	841.93	7.39%	4
			100	837.50	6.82%	7
			200	837.50	6.82%	14
			500	834.28	6.41%	32
8082	US	CVRPLib	0	971.82	23.96%	1
			50	867.72	10.68%	4
			100	796.05	1.54%	7
			200	796.05	1.54%	13
			500	787.81	0.49%	30
	CS	CVRPLib	0	917.07	16.97%	1
			50	829.60	5.82%	4
			100	829.60	5.82%	7
			200	823.85	5.08%	13
			500	791.81	1.00%	30
	US	CVRPLib	0	1016.27	29.63%	1
			50	865.31	10.37%	4
			100	865.31	10.37%	7
			200	858.44	9.49%	13
			500	858.44	9.49%	30
12175	CS	CVRPLib	0	917.09	16.98%	1
			50	811.18	3.47%	4
			100	810.27	3.35%	7
			200	806.12	2.82%	13
			500	806.12	2.82%	30

Table 24: Comparison of uniform sampling and our coreset method with training dataset CVRP100- $\mathcal{U}(0, 1)$ on test data from different distributions.

Sample size	Method	Test distribution	RRC-budget (\downarrow)	Length (\downarrow)	Gap (\downarrow)	Time (\downarrow)
128000	Org	CVRP100	0	17.35	4.64%	3
			50	16.36	-1.38%	47
			100	16.22	-2.18%	90
			200	16.13	-2.75%	170
			500	16.02	-3.40%	418
4697	US	CVRP100	0	18.48	11.43 %	3
			50	17.15	3.39%	44
			100	16.93	2.08%	85
			200	16.74	0.93%	161
			500	16.57	-0.10%	396
	CS	CVRP100	0	18.44	11.20%	3
			50	17.10	3.10%	44
			100	16.89	1.85%	85
			200	16.70	0.69%	161
			500	16.53	-0.34%	
7694	US	CVRP100	0	18.22	9.83%	3
			50	16.91	1.96%	44
			100	16.71	0.78%	83
			200	16.55	-0.21%	158
			500	16.39	-1.17%	389
	CS	CVRP100	0	18.16	9.52%	3
			50	16.91	1.97%	45
			100	16.72	0.82%	86
			200	16.56	-0.18%	162
			500	16.40	-1.10%	400
12033	US	CVRP100	0	18.03	8.70%	3
			50	16.82	1.41%	45
			100	16.64	0.34%	86
			200	16.50	-0.54%	162
			500	16.35	-1.43%	395
	CS	CVRP100	0	18.01	8.59%	3
			50	16.81	1.36%	44
			100	16.62	0.21%	84
			200	16.48	-0.64%	160
			500	16.34	-1.55%	39

Table 25: Comparison of uniform sampling and our coreset method with training dataset CVRP100- $\mathcal{N}(0, 0.1)$ on test data of varying sizes. We fix the sample size as 12033.

Sample size	Method	Test distribution	RRC-budget (\downarrow)	Length (\downarrow)	Gap (\downarrow)	Time (\downarrow)
128000	Org	CVRP200	0	22.41	11.08%	2
			50	21.20	5.08%	36
			100	21.05	4.36%	68
			200	20.93	3.76%	145
			500	20.75	2.88%	353
		CVRP500	0	41.01	10.16%	1
			50	39.69	6.61%	190
			100	39.42	5.87%	319
			200	39.16	5.20%	645
			500	38.91	4.51%	1730
			0	43.09	16.19%	73

Continued on next page

CVRP1000

Table 25: Comparison of uniform sampling and our coreset method with training dataset CVRP100- $\mathcal{N}(0, 0.1)$ on test data of varying sizes. We fix the sample size as 12033.

Sample size	Method	Test distribution	RRC-budget (\downarrow)	Length (\downarrow)	Gap (\downarrow)	Time (\downarrow)
12033			50	37.09	11.85%	904
			100	41.17	11.00%	1828
			200	40.76	9.90%	3708
			500	40.29	8.63%	9216
			0	23.29	15.45%	2
	US	CVRP200	50	21.98	8.94%	28
			100	21.75	7.82%	54
			200	21.57	6.91%	115
			500	21.33	5.72%	281
			0	20.17	14.97%	2
	CS	CVRP200	50	21.93	8.70%	29
			100	21.75	7.83%	54
			200	21.59	7.04%	116
			500	21.30	5.50%	282
			0	37.23	16.76%	2
	US	CVRP500	50	41.77	12.19%	177
			100	41.38	11.15%	296
			200	41.02	10.18%	598
			500	40.51	8.82%	1620
			0	43.19	16.02%	2
	CS	CVRP500	50	41.66	11.89%	176
			100	41.25	10.81%	295
			200	40.88	9.80%	597
			500	40.40	8.52%	1609
			0	48.20	29.96%	73
12033	US	CVRP1000	50	46.12	24.33%	907
			100	45.67	23.14%	1847
			200	45.04	21.43%	3816
			500	44.29	19.42%	9324
			0	48.24	30.05%	73
	CS	CVRP1000	50	45.89	23.73%	899
			100	45.50	22.66%	1820
			200	44.87	21.02%	3672
			500	44.07	18.82%	9180

Table 26: Comparison of uniform sampling and our coreset method with training dataset CVRP100- $\mathcal{N}(0, 0.1)$ on test data CVRPLib.

Sample size	Method	Test distribution	RRC-budget (\downarrow)	Length (\downarrow)	Gap (\downarrow)	Time (\downarrow)
128000	Org	CVRPLib	0	856.40	9.24%	1
			50	797.45	1.72%	6
			100	797.45	1.72%	10
			200	797.45	1.72%	20
			500	797.45	1.72%	47
4697	US	CVRPLib	0	902.29	15.09%	1
			50	846.35	7.95%	5
			100	838.10	6.90%	7
			200	838.10	6.90%	14
			500	838.10	6.90%	32
	CS	CVRPLib	0	1020.05	30.10%	1
			50	809.93	3.30%	4
			100	797.45	1.72%	7
			200	797.45	1.72%	14
			500	797.45	1.72%	32
8082	US	CVRPLib	0	1096.32	39.84%	1
			50	846.93	8.03%	4
			100	846.93	8.03%	7
			200	846.93	8.03%	13
			500	846.93	8.03%	32
	CS	CVRPLib	0	866.09	10.47%	1
			50	789.79	0.74%	4
			100	789.79	0.74%	7
			200	789.79	0.74%	13
			500	789.79	0.74%	31
	US	CVRPLib	0	864.85	10.31%	1
			50	830.51	5.93%	4
			100	797.45	1.72%	7
			200	797.45	1.72%	14
			500	797.45	1.72%	32
12033	CS	CVRPLib	0	965.89	23.20%	1
			50	816.14	4.10%	4
			100	809.71	3.28%	7
			200	799.16	1.93%	13
			500	787.20	0.41%	32